Computational Image Analysis Methods for the Study of Perinatal Brain Development

Andrea Urru

TESI DOCTORAL UPF / year 2022

THESIS SUPERVISORS
Miguel A. González Ballester, Gemma Piella
Department of Information and Communication Technologies

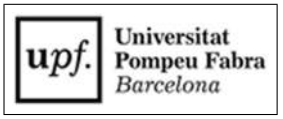

To the ones I love, and loved.

Preface

First of all, I would like to thank my supervisors Dr. Miguel Angel González Ballester, who gave me the opportunity to join this amazing group of people in the first place, and Dr. Gemma Piella, who through many difficult times helped me as much as possible. They probably have been for a while the only ones to believe I could make it to the end of this PhD. A huge part of this would not have been possible without Dr. Oualid Benkarim, who has been a tutor, friend and model for me. I admire you greatly. Finally, I would like to thank the people from Hospital Clinic for their support on the clinical aspects of this thesis, and the patients that participated in the studies.

But at the end of this journey, I would particularly like to thank all the people that helped me, without even knowing it, to get to the bottom of this. Most of them know how many times I struggled, I thought I couldn't make it, I gave up. If I am here now, it's not because I didn't give up, but just because these people didn't give up on me.

I would like to thank my colleagues, the "plebe", the beachvolley teammates and especially Amelia, which for years has been my neighbour, daily mate at work since the beginning. We have also been the best one-two punch the beachvolley tournament has seen so far, hands down. We all became a family and even if the pandemic split us up, I will keep the memories of these years together.

Thanks to all my friends who have always been a strength for me, something I could always be proud of, even when I felt miserable and empty. At least, I had them, I did something good. And indeed, I have them, and that is enough to make anyone rich.

Thanks to Laia, who has been the most important person in my life for a big part of this journey. Life is weird and unpredictable, but despite what happens between two people, great feelings leave a mark. And you definitely left a mark, indelible, and I'll keep it with me forever.

Thanks to my family, which is always with me. They made me, they know me (and they use it against me sometimes!). But I know they want me to thrive, to be happy, to be successful, because my happiness is theirs.

I wouldn't be anywhere close to the man I am without the family behind me.

Thanks to life, which unexpectedly brought you back to me. Let's not waste the opportunity.

To myself, I just want to remind that everyone fails at who they are supposed to be. The only thing that matters is how well we succeed at being who we are.

Abstract

Perinatal medicine has drawn increasing attention by the neuroscientific research community, as an early detection of most pathologies leads to more effective therapies and treatments. Monitoring fetal and neonatal brain development through brain imaging, in particular, helps studying and identifying abnormalities that commonly take place at a pre-natal stage and have effects on post-natal development. The fast-developing perinatal brain poses several challenges that the existing techniques for adult brain analysis are not able to overcome, leading to the development of specific medical image analysis techniques and methodologies. Many of these challenges, though, remain unsolved.

The purpose of this thesis is to present an automatic perinatal pipeline for segmentation and analysis of both pre- and post-natal magnetic resonance imaging (MRI) of the brain, and investigate *in* and *ex utero* brain development under specific abnormal conditions. The key contributions of this thesis are twofold: in the first part we present an automatic pipeline for fetal and neonatal segmentation and cortical mesh extraction. We propose two newly constructed temporal and multi-subject atlases, and present their application within the pipeline for atlas-based segmentation, based on novel registration methods. We extract the brain cortical mesh and compute morphometric descriptors of cortical folding, namely: mean curvature, local gyrification index, sulcal depth, and cortical thickness. We apply the pipeline to fetal and neonatal images and compare segmentation accuracy to state-of-the-art methods and ground truth. Our results show that the introduction of the new templates together with our segmentation strategy leads to accurate results when compared to expert annotations, as well as better performances when compared to available methodologies.

In the second part of the thesis, we present a longitudinal study, using a dataset of 30 subjects (15 healthy controls and 15 subjects diagnosed with ventriculomegaly (VM)), with structural MRI acquired *in* and *ex utero* for each subject. We investigated the impact of fetal VM on cortical development from a longitudinal perspective, from fetal to neonatal stage. Particularly, we studied the relationship of ventricular enlargement with

both volumetric features and a multifaceted set of cortical morphometric features including mean curvature, local gyrification index, sulcal depth, and cortical thickness. Our results show significant effects of VM on both volumetric and morphometric descriptors of cortical development in specific areas of the brain including the occipital, parietal and frontal lobes. This study shows the potential of the developed pipeline to perform innovative neuroimaging studies.

Resumen

La medicina perinatal ha atraído cada vez más la atención de la comunidad de investigación neurocientífica, ya que la detección temprana de la mayoría de las patologías conduce a terapias y tratamientos más efectivos. El seguimiento del desarrollo cerebral fetal y neonatal a través de imágenes cerebrales, en particular, ayuda a estudiar y a identificar anomalías que comúnmente ocurren en la gestación y tienen efectos en el desarrollo posnatal. El rápido desarrollo del cerebro perinatal plantea varios desafíos que las actuales técnicas para el análisis del cerebro adulto no pueden superar, lo que lleva al desarrollo de técnicas y metodologías específicas de análisis de imágenes médicas. Sin embargo, muchos de estos desafíos siguen sin resolverse.

El propósito de esta tesis es presentar un pipeline para la segmentación automática y el análisis de imágenes de resonancia magnética (IRM) del cerebro tanto prenatales como posnatales, e investigar el desarrollo cerebral *in* y *ex utero* bajo específicas condiciones anormales. Las contribuciones clave de esta tesis son dos: en la primera parte presentamos un proceso automático para la segmentación fetal y neonatal y la extracción de malla cortical. Proponemos dos nuevos atlases temporales y de múltiples sujetos, y presentamos su aplicación dentro del pipeline para la segmentación basada en atlas, con un nuevo método de registro. Extraemos la malla cortical del cerebro y calculamos los descriptores morfométricos del desarrollo cortical, en concreto: curvatura media, índice de girificación local, profundidad del surco y espesor cortical. Aplicamos el pipeline a imágenes fetales y neonatales y comparamos la precisión de la segmentación con los métodos más avanzados e imágenes segmentadas manualmente por un experto. Nuestros resultados muestran que la introducción de los nuevos atlases junto con nuestra estrategia de segmentación conduce a resultados precisos en comparación con las anotaciones de expertos, así como a un mejor rendimiento en comparación con las metodologías disponibles.

En la segunda parte de la tesis, presentamos un estudio longitudinal, utilizando un conjunto de datos de 30 sujetos (15 controles sanos y 15 sujetos diagnosticados con ventriculomegalia (VM)), con resonancia magnética

estructural adquirida *in* y *ex utero* para cada tema. Investigamos el impacto de VM fetal en el desarrollo cortical desde una perspectiva longitudinal, desde el periodo fetal hasta el periodo neonatal. En particular, estudiamos la relación del agrandamiento ventricular con las características volumétricas y distintas características morfométricas corticales que incluyen la curvatura media, el índice de girificación local, la profundidad del surco y el espesor cortical. Nuestros resultados muestran efectos significativos de VM en los descriptores volumétricos y morfométricos del desarrollo cortical en áreas específicas del cerebro, incluidos los lóbulos occipital, parietal y frontal. Este estudio muestra el potencial del pipeline desarrollado para realizar estudios innovadores de neuroimagen.

Contents

List of Figures

List of Tables

Chapter 1

INTRODUCTION

1.1 Overview

Perinatal medicine is a rapidly expanding field, as an early detection of most pathologies leads to more effective therapies and treatments D'Addario (2017). In particular, monitoring fetal and neonatal brain development has drawn increasing attention as abnormalities commonly occur already at fetal stage, typically including ventriculomegaly, abnormalities of the corpus callosum and of the posterior fossa Glenn (2010). Ventriculomegaly (VM), for instance, represents one of the most common pathologies in these early stages, and it consists of an abnormal enlargement of one or both ventricles. It has been found that the ventricular development is correlated with an abnormal development of the cortex and disfunctional behaviours, but it is unclear what is the influence of fetal VM on this kind of disorders at adult stage due to the lack of postnatal and long term follow-up studies. Moreover, typically diagnosis is based on visual inspections of the acquired images or manual measurements made by the clinician. Automatic quantification techniques are desirable over manual measurements as the latter are very time-consuming and subject to intra- and inter-rater variability. For this reason, in the last decades research has been focusing on finding automatic methodologies to accurately segment brain structures and quantitatively assess brain development, both at fetal and neonatal stage. This field presents a number of critical challenges and, although several works have been published and dramatic improvements have been made so far, many of them remain unsolved. The aim of this thesis is to contribute to the field of perinatal brain development by introducing a unique framework to analyse the whole temporal window going from pre- to post-natal, both at a single time-point and longitudinally.

1.2 Perinatal Brain Development

During gestation, the cortex gradually evolves from a smooth sheet to a highly convoluted surface, with the appearance of formations called gyri and sulci, as shown in Fig. 1.1.

Gyri, in particular, are convex formations surrounded by concave

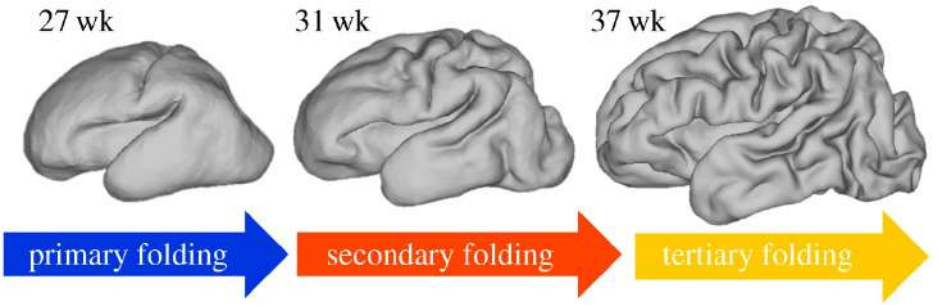

Figure 1.1: Brain development during gestation: the cortex evolves from a plain sheet to a convoluted surface.

bendings of the cortical plate called sulci. Deeper, larger sulci are called fissures, and they divide the different lobes and the two brain hemispheres. Combinations of gyri and sulci allow having a very large cortical surface, and thus a large number of neuronal connections, without the need of a proportional enlargement of the whole brain. Even though not completely understood yet, the convolution patterns of the cerebral cortex look closely related to the architectural and functional specialization of the cortical surface Fernández et al. (2016); Toro and Burnod (2005). Moreover, some studies show that the convolution pattern of the cortical plate is related with its cytoarchitecture Fischl et al. (2008). Hence, the understanding and modeling of these patterns and their regulating mechanisms have drawn increasing attention in research through the decades. What is clear from the observation of cortical maturation is that sulci formation follows consistent patterns across subjects as regards the primary sulci (e.g., the Sylvian fissure, also known as lateral sulci) Armstrong et al. (1995); Chi et al. (1977); Griffiths et al. (2010). Many theories have been developed about the reason for these consistent patterns. The first hypotheses about external constraints Clark (1945) assumed that the bending of the brain was due to the external constraint given by the size of the skull. Through the years, many works explained the mechanical folding with a differential growth of different layers of the brain Richman et al. (1975); Tallinen et al. (2016); Toro and Burnod (2005): in this hypothesis, a faster growth rate of the

outer layers compared to the inner ones forces gyrification. Other works proposed as explanation axonal tension in white matter between nearby cortical areas Essen (1997); Hilgetag and Barbas (2006) and differential proliferation of neural progenitors Kriegstein et al. (2006). As regards the smaller, more superficial secondary and tertiary sulci, more irregular patterns regulate their formation. Whereas at the end of gestation primary sulci are already formed, they continue to develop from fetal to neonatal stage Voorhies et al. (2021) and different, complementary theories have been proposed Lefèvre and Mangin (2010); Welker (1990) to model their constitution.

Understanding the mechanics beneath cortical development could help improve both diagnosis and treatments in case of abnormal growth. An abnormal development of the cortex, in fact, could be the outcome of a pathological situation, such as in case of ventriculomegaly Benkarim et al. (2020, 2018a); Kyriakopoulou et al. (2014); Scott et al. (2013), and can cause disorders such as schizophrenia, autism, lissencephaly and attention deficit in adults Jou et al. (2005); Landrieu et al. (1998); Nordahl et al. (2007); Sallet et al. (2003); Wolosin et al. (2009). Ventriculomegaly (VM) is one of the most common pathologies in fetuses and neonates, as it involves around 1% of pregnancies Huisman et al. (2012); Salomon et al. (2007). This pathology affects one or both ventricles and it is generally defined by an atrial diameter higher than 10mm, at fetal stage (from 14 gestational weeks onwards). It has been found that an abnormal ventricular development is correlated with cortical overgrowth at fetal stage Benkarim et al. (2018a); Kyriakopoulou et al. (2014) and disfunctional behaviours in neonates Hahner et al. (2019), while it is unclear what is the influence of VM on this kind of disorders at adult stage due to the lack of postnatal and long term follow-up studies. In case of diagnosed fetal VM the postnatal prognosis depends, however, on the presence of other abnormalities or a severe ventricular dilation: in case of isolated non-severe ventriculomegaly (INSVM) the subject is unlikely to be affected by long-term neurodevelopmental problems Griffiths et al. (2010); Melchiorre et al. (2009). This situation is defined by a ventricular atrium diameter between 10 and 15 mm, and it can be further classified as mild (10 to 12 mm) or moderated

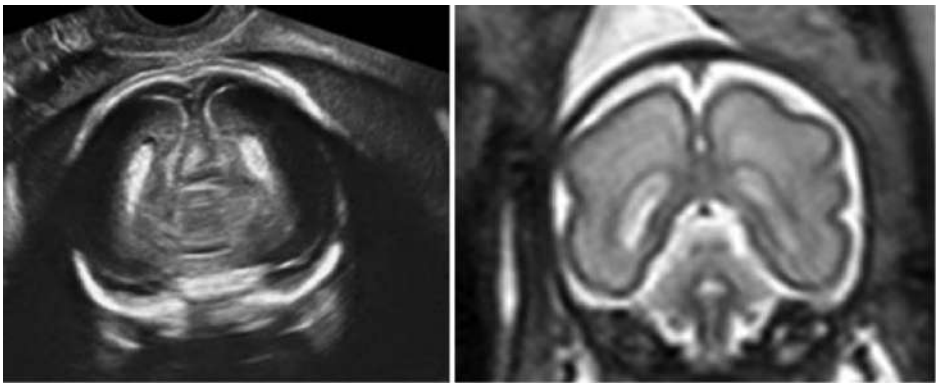

Figure 1.2: Comparison between fetal acquisitions performed using ultrasound and magnetic resonance respectively.

(12 to 15 mm). Diagnosis is usually performed by an expert based on 2D scans of the neonatal brain: this kind of diagnosis is obviously affected by intra- and inter-rater variability which could be overcome by an objective classification system.
It is then of utmost importance to accurately monitor and quantify the brain growth particularly from the third trimester of gestation on, as in this phase the brain undergoes most of its functional development: specific acquisition tools and analysis methods are used to do that, and in the next sections we will go through them in relation with their use in the field.

1.3 Perinatal Brain Imaging Techniques

Perinatal, non-invasive imaging by means of different techniques such as ultrasonography (US) and magnetic resonance imaging (MRI) has drawn increasing attention for clinical purposes, as they allow monitoring the development of different brain tissues and structures Dubois et al. (2021); Griffiths et al. (2019); Milani et al. (2019) both in utero and ex utero. A comparison of the two techniques is shown in Fig. 1.2.

Pregnancies are periodically monitored using US and fetal MRI has become a very important tool as it is performed to evaluate the brain

in cases where an abnormality is detected with US. After birth, on the other hand, MRI can be used to monitor the correct development of the newborn's brain. Thus, an accurate acquisition of the in utero and ex utero brain plays a crucial role in clinical decision-making and neuroscience research.

For decades, US has been recognised as the primary technology in fetal brain imaging Garel (2008). The acquisition of real-time images and the relatively low cost represent the main advantages of US. There are limitations, however, particularly in cases of reduced amniotic fluid volume, maternal obesity, inappropriate fetal head position, multiple pregnancy, and bony reverberation artifacts from the skull Glastonbury and Kennedy (2002); Twickler et al. (2003). Studies conducted in the past have found that the rate of detection of brain abnormalities overlooked by ultrasound has been up to 50% Garel (2008).

MRI, on the other hand, is the most common medical imaging modality for the diagnosis and follow-up of patients with brain abnormalities, and the understanding of normal neurodevelopment in neonatal and adult brains. With respect to US, MRI offers superior contrast in soft tissues and an increased field of view, which makes it suitable also for pre-natal application. Prenatal diagnosis therefore benefits from fetal MRI by complementing the findings of the low-cost, less invasive US screening. Indeed, in recent years, in utero MRI has shown to be of important added value in the study of disorders Clouchoux et al. (2013); Kyriakopoulou et al. (2014); Scott et al. (2013) and early brain development Clouchoux et al. (2012); Wright et al. (2014).

In neonates and infants, 1.5-3T MRI scanners are commonly used. In fact, despite higher associated radiofrequency radiation, 3T MRI does not induce any significant increase in temperature Cawley et al. (2016) and it does not endanger the newborn. Nevertheless, this kind of image acquisition introduces multiple constraints that make studying brain development at this stage more challenging than looking at the adult brain. For example, infants are not sedated without a specific clinical indication and this introduces motion artifacts when acquiring the image: as a solution to this issue, short acquisition sequences or motion-tolerant acquisition and re-

construction approaches can be used. The small size of the brain structures is also an issue with respect to adult brain imaging: increasing the image spatial resolution is required to avoid partial voluming (PVE) Kneeland et al. (1986); Simmons et al. (1994). PVE is present when multiple tissues contribute to a single voxel producing a blurring effect, for instance, in the boundary between gray matter (GM) and cerebrospinal fluid (CSF), and can lead to volume measurement errors in the range of 20%-60% González Ballester et al. (2002). Besides, incomplete maturation of the infant's brain leads to different tissue characteristics than those of the adult brain, thus requiring non-standard MRI protocols (e.g., relaxation times: longitudinal relaxation time T1, transverse time T2) to avoid signal inhomogeneity and deal with the contrast specificity of newborn images.

In fetuses, the identification and reconstruction of the brain from MRI is even more challenging than that of the ex utero brain. Proper acquisition of full 3D MRI of the fetal brain is difficult due mainly to the thick slice acquisition necessary to achieve good signal-to-noise ratio (SNR) and the presence of motion artifacts caused by spontaneous movement of the fetus and maternal breathing. Shortening the acquisition time would help decrease the likelihood of motion artifacts Malamateniou et al. (2013). To mitigate the effect of fetal and maternal motion, fast imaging methods such as single-shot spin echo are used to acquire thick, low-resolution stacks of 2D slices that can largely freeze in-plane motion Saleem (2014) and in conjunction with post-processing techniques (i.e., motion correction and super resolution) are used to reconstruct the brain in 3D space. Typically, several motion-corrupted stacks of thick 2D slices are acquired in orthogonal orientations and then combined to obtain a high resolution motion-free 3D volume of the brain. Some existing methods for motion correction and reconstruction Kim et al. (2009); Kuklisova-Murgasova et al. (2012) require the delineation of the fetal brain (at least in one slice) from maternal tissue. In Keraudren et al. (2014) a fetal brain extraction method from 2D stacks is proposed, that combined with the reconstruction approach in Kuklisova-Murgasova et al. (2012) provides a fully automated pipeline to obtain the final 3D volumes. Recently, a convolutional neural network (CNN) based super-resolution reconstruction methodology has

been proposed Ebner et al. (2018a, 2019, 2018b), introducing an automatic localization of the brain in each stack and a new methodology for outlier rejection.

1.4 Perinatal Brain Analysis Tools

Quantitative measurements of brain structures and cortical surface are important to characterise brain development as they could be useful to predict neurodevelopment in the medium to long term Boardman et al. (2010); Counsell et al. (2008); Peterson et al. (2003); Rathbone et al. (2011); Thompson et al. (2008). Nonetheless, manual segmentation of structural MRI is very time consuming. Furthermore, manual labelling is subject to inter- and intra-rater variability, which limits its reproducibility. These limitations become important when labelling a large number of subjects required for population studies: for this purpose, automated segmentation algorithms have drawn a lot of attention in research, to achieve accurate and reproducible parcellation of brain structures, rather than manual segmentations provided by an expert. However, as highlighted above, the brain at this stage is rapidly evolving both in terms of internal structures and externally on the cortical surface, going from a rather flat sheet to a highly convoluted structure, making automatic segmentation of the neonatal and fetal brain considerably more challenging than it is in adults. Structural MRI of the perinatal brain, compared to adult brain, has a much lower contrast-to-noise ratio (CNR) Prastawa et al. (2005), lower signal-to-noise ratio (SNR) due to the small size of the brain and may vary dramatically in terms of brain shape and appearance across subjects and time, as a result of rapid brain development during this period. Moreover, it is further subject to significant motion artifacts during the image acquisition, both pre- and post-natal. As previously mentioned, there are other significant challenges in perinatal MRI that represent an obstacle to the successful creation of automatic segmentation algorithms. The intensity of the different tissues is not uniform, presenting gradual changes over the image space. This intensity inhomogeneity is caused by non-uniform radio-frequency fields

and reception sensitivity as well as electromagnetic interaction with the body Belaroussi et al. (2006) . Algorithms such as the N3 Sled et al. (1998) and the N4 Tustison et al. (2010b) can be leveraged prior to the segmentation to compensate for these inhomogeneities. The aforementioned PVE, the mixing of different tissue classes in a single voxel, introduces additional difficulties for the accurate delineation of the tissue boundaries. Since the image resolution is limited, voxels that contain more than one tissue result in an intensity that represents the mixture of tissues in the voxel. In particular, perinatal MRI shows an inverted contrast between white matter (WM) and grey matter (GM) compared to the adult brain images. Due to a not complete myelination, the WM in the perinatal brain appears brighter than GM in the T2- weighted images. The mixing of cerebrospinal fluid (CSF) and cortical GM (CGM) at the boundary leads to intensities similar to the intensity profile of the WM, leading to mislabelled voxels in the CSF-CGM interface Xue et al. (2007). The last 20 years have seen an increasing number of works in this subject, as well as the emergence of large-scale projects targeting fetuses and neonates, such as the developing Human Connectome Project (dHCP) Makropoulos et al. (2018).

Most of the methods developed so far aim to label either the whole brain, different tissues or local structures and substructures in fetal or neonatal brains. Following the criteria of Makropoulos et al. (2017), the segmentation techniques proposed so far for brain MR images can be divided in five main groups based on the methodology they adopt: unsupervised, atlas fusion-based, parametric, classification-based, deformable model-based. The developed methods available in literature divided by perinatal stage (i.e., fetal or neonatal), type of segmentation (i.e., brain, tissue or structural) and the five categories previously named are schematised in Figure 1.3 and described in detail in Chapter 2.

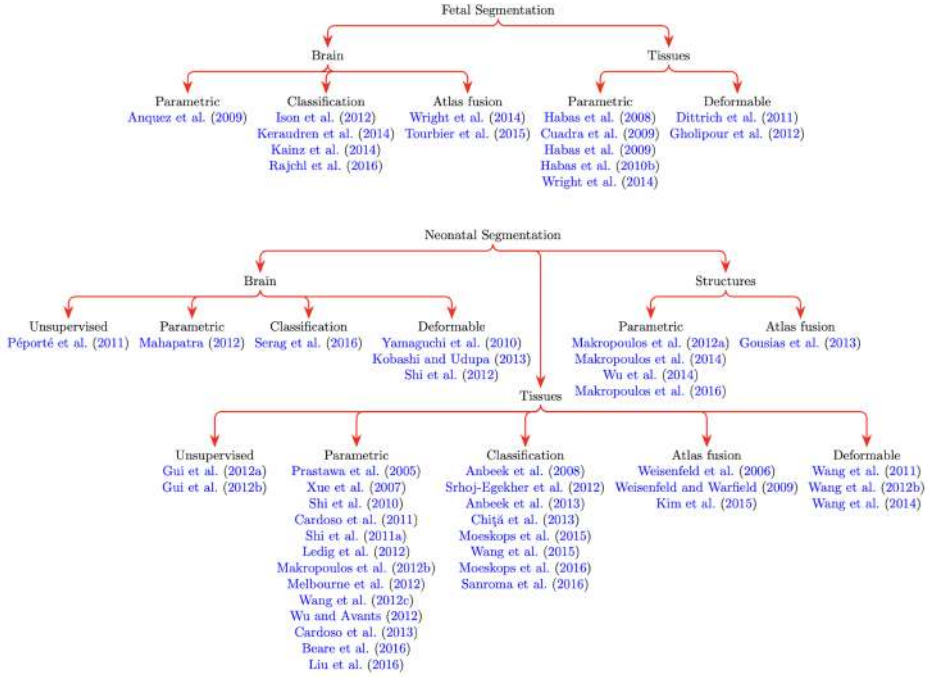

Figure 1.3: Segmentation methods divided by category as presented in Makropoulos et al. (2017).

1.5 Thesis Summary

This thesis aims to contribute in the field of fetal and neonatal analysis by presenting a newly developed automatic segmentation pipeline for different perinatal stages, including the early and late gestational period and the neonatal period, and an application of the developed segmentation pipeline for a longitudinal analysis of perinatal brain development in VM. In the first part, the methodologies used to build the pipeline are presented.
We first review the state of the art of related algorithms (e.g. Benkarim et al. (2017); Makropoulos et al. (2017)). Based on these techniques, pipelines for the automatic segmentation of fetal and neonatal brains have been

developed, but they all present different limitations. The dHCP pipeline Makropoulos et al. (2018) aims to build a neonatal brain connectome starting from the acquired structural MRI, but it does not tackle the challenges of fetal acquisition, reconstruction and segmentation. In general, in the existing works there is a lack for longitudinal studies and tools. The atlases developed so far for fetal and neonatal development present different parcellations, which makes comparison between pre- and post-natal segmentations difficult Gholipour et al. (2017); Kuklisova-Murgasova et al. (2011); Serag et al. (2012a). As regards structural segmentation, although the atlases in Gousias et al. (2012); Makropoulos et al. (2016) propose a regional labeling for neonatal brain, there is not an equivalent multi-subject atlas for fetal brains. In Payette et al. (2020) an annotated dataset composed of 50 fetal brains is used to compute a tissue segmentation by supervised learning techniques and multi-subject atlas segmentation. It focuses on prenatal segmentation, but it does not integrate the brain super-resolution reconstruction (SRR) and skull extraction as a preprocessing part. Moreover, only the tissue segmentation is computed, no structural or regional information and no cortical surface mesh estimation is given. The presented pipeline aims to tackle these gaps by introducing (a) a new fetal multi-tissue segmentation based on Gholipour et al. (2017) brain spatio-temporal probabilistic atlas; (b) a newly developed multi-subject fetal atlas, used for tissue and structural segmentation; (c) a super-resolution reconstruction, using a 2D U-net based skull stripping method Salehi et al. (2018) and the super-resolution reconstruction presented in Ebner et al. (2019), added as a pre-processing step to the pipeline; (d) structural and multi-tissue segmentations computed through a multi-channel, multi-resolution non-linear registration to the developed templates using ANTs toolbox Avants et al. (2009). The pipeline is built upon the existing dHCP pipeline Makropoulos et al. (2018) for neonatal segmentation, with increased performances in terms of segmentation accuracy in case of fetal acquisition and computational load.

In the second part, this pipeline is used to compute the tissue and regional segmentation and to extract the cortical surfaces in a longitudinal dataset of 30 subjects (15 healthy controls and 15 subjects diagnosed with VM).

With structural MRI acquired in and ex utero for each subject, we sought to examine the impact of fetal VM on both pre- and postnatal cortical development. Particularly, we investigated the relationship of ventricular enlargement and VM diagnosis not only with cortical volume, but with single lobular volume and with a multifaceted set of cortical folding measures, namely: local gyrification, sulcal depth, curvature and cortical thickness. These features represent different developmental characteristics of the cortex. With our analysis, we go from a global analysis looking at macro structural volumes and average feature values throughout the cortex, through an analysis of the relationship between lobular volume and diagnosis, to a vertex-wise analysis of the aforementioned cortical features. We do this not only at each time-point (i.e., fetal and neonatal stage), but rather longitudinally by means of generalised linear models (GLMs) which allow to take into account multiple acquisitions of the same subjects. Our findings not only confirm the cortical overgrowth in VM subjects longitudinally, but show also a correspondence between the cortical overgrowth in INSVM subjects and an abnormal development represented by higher values of thickness and reduced gyrification, both globally and in some specific areas of the brain.

Chapter 2

AN AUTOMATIC PIPELINE FOR ATLAS-BASED FETAL AND NEONATAL BRAIN SEGMENTATION AND ANALYSIS

Abstract – The automatic segmentation of perinatal brain structures in magnetic resonance imaging (MRI) is of utmost importance for the study of brain growth and related complications. While different methods exist for adult and pediatric MRI data, there is a lack for automatic tools for the analysis of perinatal imaging. In this work, a new pipeline for fetal and neonatal segmentation has been developed. We also report the creation of two new fetal atlases, and their use within the pipeline for atlas-based segmentation, based on novel registration methods. The pipeline is also able to extract cortical and pial surfaces and compute features, such as curvature, thickness, sulcal depth, and local gyrification index. Results show that the introduction of the new templates together with our segmentation strategy leads to accurate results when compared to expert annotations, as well as better performances when compared to a reference pipeline (developing Human Connectome Project (dHCP)), for both early and late-onset fetal brains. The pipeline's source code and atlases, as well as its installation and usage guidelines are publicly available at `https://github.com/urrand/perinatal-pipeline`.

This chapter is adapted from:
A. Urru A., Nakaki A., Benkarim O. M., Crovetto F., Segales L., Comte V., Hahner N., Eixarch E., Gratacós E., Crispi F., Piella G., González Ballester M. A., An automatic pipeline for atlas-based fetal and neonatal brain segmentation and analysis. *Submitted to IEEE Access*, 2022.

2.1 Introduction

Perinatal brain imaging has drawn increasing attention for clinical purposes, as many diseases can be identified already at fetal or neonatal stage by monitoring the development of different brain tissues and structures Benkarim et al. (2020, 2018a); Hahner et al. (2019); Jackson et al. (2011); Wright et al. (2000). Early diagnosis of abnormal development has thus revealed to be of utmost importance for improved treatments and follow-up. Advances in imaging techniques such as Magnetic Resonance Imaging (MRI) made it possible to obtain highly detailed 3D images of the brain. Compared to the adult brain, however, perinatal brain MRI encounters a number of non-trivial challenges, among which increased motion artifacts, especially in fetal MRI, temporal variations in tissue intensities, low contrast-to-noise ratio and the high growth rate of the brain in this period, which makes monitoring its development through time more difficult. Although being largely investigated, this topic remains an open challenge in image analysis Benkarim et al. (2017).

This work introduces the first segmentation pipeline aimed at seamlessly addressing the analysis of the whole perinatal period, both pre- and post-natal. Over the years, several algorithms have been proposed for fetal or neonatal image analysis (see Benkarim et al. (2017); Makropoulos et al. (2017) for reviews); however, the methods developed so far present different limitations. In particular, they aim to label the whole brain, different tissues or local structures and substructures in fetal or neonatal brains. Nevertheless, there is a lack for an end-to-end tool for an automated analysis of both fetal and neonatal acquisitions, which would allow for a more advanced and complete analysis of the brain development, combining an automatic tissue segmentation to a regional, structural segmentation.

Related works include the dHCP pipeline Makropoulos et al. (2018), which aims to build a neonatal brain connectome starting from the acquired MRI, but does not tackle the challenges of fetal acquisition, segmentation and reconstruction. In Payette et al. (2020) an annotated dataset composed of 50 fetal brains is used to compute a tissue segmentation by supervised learning techniques and multi-atlas segmentation. It focuses on prenatal

segmentation, but it does not integrate the brain super-resolution reconstruction (SRR) Ebner et al. (2019) and skull extraction as pre-processing steps. Moreover, only the tissue segmentation is computed; no structural or regional information and no cortical surface mesh estimation are generated.

In this work, a newly developed framework for fetal and neonatal segmentation and analysis is proposed. The pipeline is built upon the existing dHCP pipeline Makropoulos et al. (2018) for neonatal segmentation, and it introduces:

1. A new fetal multi-tissue segmentation based on the brain spatio-temporal probabilistic atlas Gholipour et al. (2017).

2. A newly developed multi-subject fetal atlas, built from new data acquired at our institution, and its application for tissue and structural segmentation. This atlas, shared to the community, is in itself an important contribution to the field.

3. For fetal acquisitions, highly affected by motion-related noise, a super-resolution reconstruction, using a 2D U-net based skull stripping method Salehi et al. (2018) and the NiftyMIC SRR framework Ebner et al. (2019), added as a pre-processing step to the pipeline.

4. Structural and multi-tissue segmentation, computed through a multi-channel, multi-resolution non-linear registration to the developed templates, using the ANTs toolbox Avants et al. (2009).

5. The pipeline's source code and atlases, as well as its installation and usage guidelines are publicly available at `https://github.com/urrand/perinatal-pipeline`.

We next provide background information about brain segmentation methods, as well as about fetal and neonatal atlases. Then, we describe the overall structure of the pipeline and elaborate on its different elements. We present its use on a clinical dataset composed of a total of 150 fetal subjects and 30 neonates. The method shows good performance, both in

terms of visual inspection and through quantitative experiments reporting the Dice score with respect to ground truth segmentations. Furthermore, we present experiments comparing our method with the original dHCP pipeline Makropoulos et al. (2018), and show increased performance in terms of segmentation accuracy. Finally, discussions and potential directions for future research are described.

2.2 Background

2.2.1 Brain segmentation techniques

Following the criteria of Makropoulos et al. (2017), the segmentation techniques proposed so far for brain MR images can be divided in five main groups based on the methodology they adopt: unsupervised, parametric, classification-based, deformable models, and atlas fusion methods.

Unsupervised techniques often leverage traditional segmentation algorithms (e.g. thresholding, region growing, morphological operations) and are not based on previously labelled training data. They are typically highly sensitive to noise. They can be used to correct for partial volume voxels, or as a tool to compute tissue priors Makropoulos et al. (2018); Xue et al. (2007). Parametric techniques propose a segmentation by fitting a model, typically a Gaussian Mixture Model (GMM), to the data using an Expectation-Maximization (EM) approach González Ballester et al. (2000); Makropoulos et al. (2012); Van Leemput et al. (1999); Xue et al. (2007). Classification techniques use a classifier trained on a given dataset to learn how to assign a certain label to voxels or groups of voxels, based on selected features. Previous works in literature used k-NN, decision forests and, lately, convolutional neural networks (CNNs) for both brain extraction Kainz et al. (2014); Keraudren et al. (2014); Rajchl et al. (2016); Serag et al. (2016) and tissue classification Moeskops et al. (2016); Sanroma et al. (2016). Deformable models aim to segment an object via deformation of a surface based on physical internal and external energies that move locally the surface depending on the properties of the image. The external energy is usually driven by the image properties, while the in-

ternal force is used to smooth and constrain the resulting deformation. An example of deformable model-based technique is used for brain extraction and constitutes the core of the Brain Extraction Tool (BET) Smith (2002).

Finally, another group of techniques use atlases Gholipour et al. (2017); Habas et al. (2010); Kuklisova-Murgasova et al. (2011); Oishi et al. (2011); Sanroma et al. (2018); Schuh et al. (2014); Serag et al. (2012b,c), which provide a representation of the average tissue distribution and its variability in the population. The segmentation is obtained by registering the target image to the atlas. Once the alignment has been performed, label information is transferred from the atlas to the target image. Multi-subject atlases are composed of different subjects instead of a single one, representing the population. In this case, the target image is registered to each subject composing the atlas and once the alignment is performed, label information is transferred from the different subjects through a weighted average. Multi-subject atlas fusion can be used both for brain extraction Tourbier et al. (2015) and tissue or structural segmentation Gousias et al. (2013a).

2.2.2 Fetal and neonatal atlases

In the context of fetal and neonatal brain analysis, construction of corresponding atlases has been of paramount importance because they have been used not only to represent the average growth of the brain and its variation across the population, but also to automatically segment single subjects at different developmental stages Gholipour et al. (2017); Serag et al. (2012c). Currently, perinatal brain atlases can be classified in two main categories: probabilistic atlases and multi-subject atlases. Both approaches have been introduced to overcome the limitations of single-subject atlases Oishi et al. (2011), which are based on a subject taken as a reference for the population, regardless of the inherent variability in shape, size and growth rate of the brain at this stage of development.

Probabilistic atlases present a brain resulting from the average of the intensity images and segmentations of all the subjects in the cohort. In several works present in literature, a spatio-temporal probabilistic atlas is built using non-parametric kernel regression Habas et al. (2010); Kuklisova-

Murgasova et al. (2011); Schuh et al. (2014); Serag et al. (2012b). Although these works have a similar approach to compute a high-definition average of the subjects in the cohort for each time-point, they differ in the registration technique used to align the subjects: either a simple affine registration Kuklisova-Murgasova et al. (2011), a non-rigid pairwise registration between all the subjects Schuh et al. (2014); Serag et al. (2012b), or a groupwise registration Habas et al. (2010). Other works aimed to enhance these atlases, adding new labelled structures to the ones initially proposed Makropoulos et al. (2016). To obtain the segmentation for a new subject, this is registered to the template and the corresponding segmentation is computed using the resulting transformation. Since the template is smoothed out by the average, the registration is more accurate and less challenging than a registration between two individual subjects. To take into account variability across the population, probability maps for different tissues can be built, indicating for each voxel in the template its probability of belonging to each structure, or tissue.

Multi-subject atlases are another solution to represent, up to a certain extent, variability across the population; in this case, a new subject is registered to each one of the volumes in the atlas independently, and transformations are averaged out to obtain the final segmentation for the subject. Most atlases present in literature are composed of healthy Alexander et al. (2017); Gousias et al. (2012), although a dataset composed by both normal and pathological fetal brains Payette et al. (2021) has been proposed and used in different recent research works de Dumast et al. (2020); Payette et al. (2020).

Limitations in this field are related to the different segmentations proposed by each atlas, which makes comparison between pre- and postnatal segmentations difficult. Well established atlases such as Gholipour et al. (2017); Kuklisova-Murgasova et al. (2011); Serag et al. (2012a) present different segmentations of the same brain tissues. As regards structural segmentation, although the atlases in Gousias et al. (2012); Makropoulos et al. (2016) propose a regional labeling for neonatal brain, there is not an equivalent multi-subject atlas for fetal brains.

2.3 Methodology

The workflow of the proposed pipeline is summarised in Fig. 2.1. It takes as an input the raw data of the image to be segmented (fetal or neonatal). For fetal acquisitions, SRR is applied, in order to combine the different imaging stacks into one high-resolution image volume. Skull extraction and the N4 bias correction are then applied. The tissue priors for gray matter and ventricles are computed registering the obtained T2-weighted reconstructed image to the temporal templates, and they are used with the T2 image in a 3-channel registration to the structural multi-subject atlases, to obtain the tissue and structural labels. Finally, starting from the pial and white matter boundaries, the cortical surface is extracted.

All these steps are described in more detail in the subsections below. First, we will describe the imaging datasets and the atlases built and used by our pipeline.

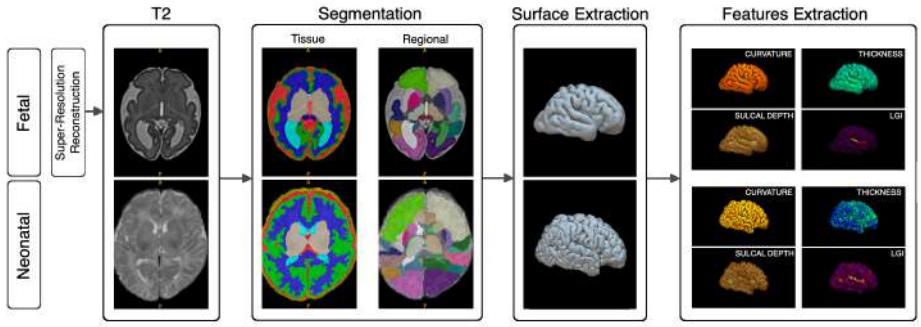

Figure 2.1: Perinatal pipeline workflow.

2.3.1 Dataset acquisition and reconstruction

Fetal Dataset

The subjects used for the fetal brain MRI dataset of this study were randomly selected pregnant participants who participated in a large randomized clinical trial Crovetto et al. (2021). All fetuses included in this study

did not have any major malformation. All participants provided written informed consent on the day of recruitment for the fetal MRI. The protocol was approved by the Ethics Committee of Hospital Clínic Barcelona, Spain (HCB/2020/0267). A total of 200 participants underwent fetal MRI between 32 weeks and 39 weeks of gestational (mean 36.5 $\pm$ 1.0 weeks SD), with the proportion of 105 (52%) male fetuses.

Single-shot fast spin-echo T2-weighted was performed on two 3.0 T MR scanners (Philips Ingenia and SIEMENS MAGNETOM Vida) in two hospitals (Hospital Sant Joan de Déu and Hospital Clínic), respectively, using a body array radio-frequency coil without sedation. The parameters used for each machine were as follows: 1) Philips: repetition time 1570 ms, echo time 150 ms, slice thickness 3 mm, field of view 290 $\times$ 250 mm, voxel spacing 0.7 $\times$ 0.7 $\times$ 3.0 mm, no interslice-slice gap; 2) Siemens: repetition time 1390 ms, echo time 160 ms, slice thickness 3 mm, field of view 230 $\times$ 230 mm, voxel spacing 1.2 $\times$ 1.2 $\times$ 3.0 mm, no interslice-slice gap. Three orthogonal planes, oriented along the axis of the fetal brainstem, obtaining 2-loops of axial, 2-loops of coronal and 2-loops of sagittal single shoot slices were obtained for each subject. Among the 200 participants, 91 underwent MRI in Hospital Sant Joan de Déu between 32 to 39 weeks of gestation (mean 36.5 $\pm$ 1.1 SD), and 109 in Hospital Clínic between 35 to 39 weeks of gestation (mean 36.3 $\pm$ 0.7 SD).

Neonatal Dataset

The 30 subjects used for the neonatal dataset of this study were part of a prospective study about fetal ventriculomegaly. Babies were scanned at 43.58 $\pm$ 1.56 weeks post-menstrual age (PMA), during natural sleep using a TIM TRIO 3.0 T whole body MR scanner (Siemens, Germany). The study protocol and the recruitment and scanning procedures were approved by the Institutional Ethics Committee, and written informed consent was obtained from the parents of each child to participate in the research studies (HCB/2014/0484). T2 weighted images were obtained with the following parameters: 2-mm slice thickness with 2 mm interslice gap, in-plane acquisition matrix of 256 $\times$ 256, FoV=160 $\times$ 241 mm, which

resulted in a voxel dimension of 0.625 $\times$ 0.625 $\times$ 2 mm, TR=5980 ms and TE=91 ms. All acquired MRI images were visually inspected for apparent or aberrant artifacts and brain anomalies and subjects excluded accordingly.

2.3.2 Atlases

In order to cover the complete perinatal period, both neonatal and fetal atlases are needed. As our pipeline is based on the dHCP pipeline Makropoulos et al. (2018), we use their atlases for neonatal data. For fetal data, however, new atlases need to be developed. In the following subsections we describe how these fetal atlases have been built, both for the temporal template and the multi-subject atlas (based on a new in-house fetal dataset).

Fetal temporal template

In the dHCP pipeline, a neonatal temporal template Serag et al. (2012a) is used to estimate the initial tissue segmentation. This template was constructed using T1 and T2 weighted MR images from 204 premature neonates (no preterm babies had visually obvious pathology). The age range at the time of scan was 26.7 to 44.3 weeks of gestation, with mean and standard deviation of 37.3 $\pm$ 4.8 weeks. All subjects were born prematurely, with mean age at birth 29.2 $\pm$ 2.7, in a range between 24.1 to 35.3 weeks of gestation. The result is a temporal template covering gestational ages between 28 and 44 weeks, and the segmentation identifies 6 tissues and the background (and additionally, it distinguishes high and low intensity white matter). The atlas and the corresponding segmentation is shown in Figure 2.2a.
In this work, an enhanced version of Gholipour et al. (2017) for tissue segmentation has been added to the pipeline for fetal segmentation. This atlas has originally been built from T2 weighted MR images of 81 healthy fetuses scanned at a gestational age range between 19 and 39 weeks, with mean and standard deviation of 30.1 $\pm$ 4.5 weeks; for each week, an average shape is computed. Two types of segmentation are proposed, one

identifying the tissues and the other, based on Gousias et al. (2012), brain structures and regions, for a total of 124 labels. In order to identify the equivalent 7-tissues segmentation, this atlas is registered to the neonatal template: each of the computed average brains composing the fetal template is registered to every average brain in the neonatal one, and the final segmentation is computed as a locally weighted average of the neonatal atlas segmentation, based on the local similarity after the registration. For the registration, the ANTs toolbox Avants et al. (2009) has been used combining a rigid, affine and non-rigid registration in a multi-resolution approach, with mutual information selected as similarity metric. A multi-channel registration has been implemented, in which the T2-weighted image, the cortical gray matter and ventricles ground truth segmentations are used to improve the registration accuracy. A few samples from the atlas and the original tissue segmentation are shown in Figure 2.2b. Once registration is performed for every time-point in the neonatal template

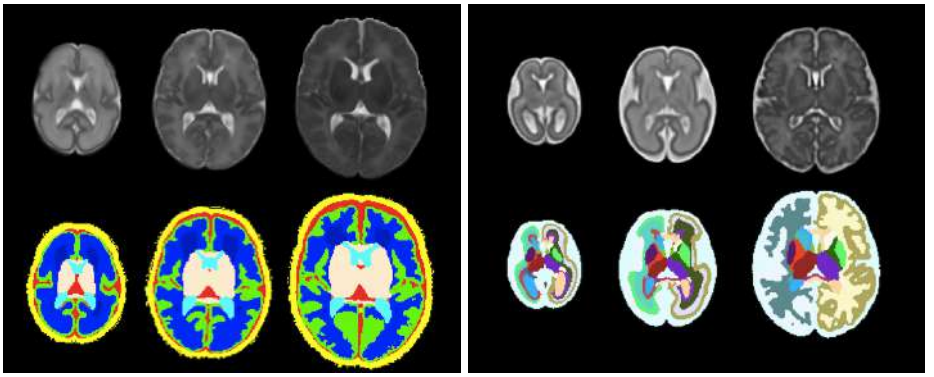

(a) (b)

Figure 2.2: Neonatal and Fetal temporal templates with corresponding original segmentations. (a) Neonatal template at 28, 36 and 44 weeks of gestation respectively. (b) Fetal template at 19, 29 and 39 weeks of gestation respectively.

with respect to each time-point of the fetal template, the correspondence between fetal and neonatal labels is established by simple majority voting

among the registered samples. Simple majority voting assigns a label and a probability for every voxel based on the most frequent class assignment, whereas the voxel is not initially classified in case of ties. Subsequently, a label is assigned to these unclassified voxels based on a weighted majority voting among the 26-connected neighborhood with their probabilities.

Multi-subject fetal atlas

In order to compute a structural segmentation for a neonatal subject, in the dHCP pipeline the ALBERTs atlas Gousias et al. (2012, 2013b) is used. This multi-subject atlas is composed of 20 manually labelled subjects and provides T1 and T2 images accompanied by the label map for each subject. 15 of the 20 subjects were born prematurely at a median age at birth of 29 weeks (range 26-35 weeks). These were scanned at term at a median age of 40 weeks (range 37-43 weeks) and had a median weight of 3.0 kg (range 2.0-4.0 kg) at the time of scan. The remaining 5 subjects were born at term at a median age of 41 weeks (range 39-45 weeks), and had a median weight of 4.0 kg (range 3.0-5.0 kg).
In this work, a corresponding dataset of $N = 20$ fetal subjects has been selected from our cohort to replicate the function of neonatal ALBERTs template for the fetal cases. As a first step, the N subjects' T2-weighted images have been selected within the cohort to maximise variability in terms of age, brain development and shape. These subjects were scanned at a median age of 36.6 weeks (range 33-38 weeks).
After a pre-processing phase consisting of intensity inhomogeneity correction Tustison et al. (2010a) and skull extraction Smith (2002), each subject is initially segmented using the fetal atlas previously described. In this case, a pairwise intensity-based registration is performed selecting the closest sample in the atlas in terms of gestational age, and the segmentation is computed based on the registration outcome. The resulting tissue segmentation has been refined by an expert and constitutes the ground truth segmentation.
Subsequently, in order to replicate the function of ALBERTs atlases, the same structural segmentation is needed. To compute it for the selected

subjects, they have been segmented using ALBERTs atlases to obtain a first estimate of their structural segmentation, using a three-channel registration with the T2-weighted images and the gray matter and ventricle segmentations. Next, each of the N subjects has been segmented using $N-1$ subjects composing the multi-subject atlas (all the subjects in the dataset but the subject analyzed) to refine their structural segmentation. The resulting structural segmentation for each subject is iteratively refined until convergence. The process is summarized in Figure 2.3.

2.3.3 Segmentation

We next describe the full processing pipeline (Fig. 2.1), which uses the atlases described above to perform segmentation on both fetal and neonatal data. For the case of fetal data, the 3D volume has to be reconstructed first from the different acquisitions along three orthogonal axes. In our pipeline, SRR is implemented Ebner et al. (2019, 2018b) to obtain the 3D image of the fetal brain. Segmentation proceeds with a brain-extraction step, implemented using BET Smith (2002), in order to remove the remaining non-brain tissue. Indeed, in neonates the skull, eyes and other structures are present in the image, whereas in fetuses sometimes parts of the skull or even the mother uterus are visible after the reconstruction. BET segments the brain tissue and cerebrospinal fluid (CSF), and removes most of the skull. Once the brain has been extracted, it is rigidly registered to the temporal templates using principal components. The pre-processing phase ends with the intensity inhomogeneity correction using the N4 algorithm Tustison et al. (2010a).
Subsequently, segmentation is performed with an Expectation-Maximization algorithm. With respect to the dHCP pipeline, we have chosen a different approach for registration in order to reduce the required computational load. In particular, in the dHCP pipeline the subject T2-weighted image is registered to each one of the subjects composing the multi-subject atlas (i.e., a total of 20 multi-resolution registrations using the ALBERTs multi-subject atlas). Here, we reduce the amount of required registrations to one. That is done by computing a single template for the multi-subject atlas and by

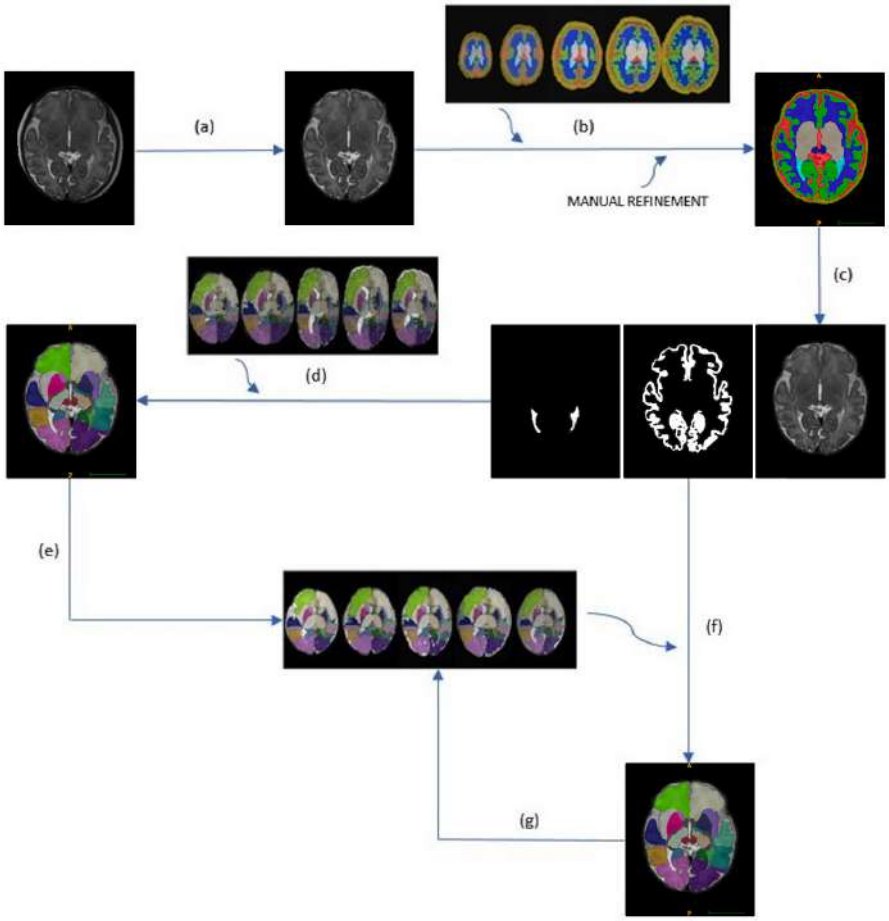

Figure 2.3: The process to generate the multi-subject fetal atlas starts from the reconstructed T2-weighted images. A pre-processing phase (a) consisting of N4 bias correction and brain extraction is performed first, followed by the tissue segmentation (b) using the modified fetal template and a manual refinement. From the obtained segmentation, gray matter and ventricles segmentation are extracted (c). They are used in a three-channel registration with the ALBERTs atlas (d) to obtain a first estimate of their structural segmentation and generate the multi-subject atlas (e). Each subject is then segmented iteratively using the other 19 subjects (f) of the atlas until convergence, and at each step the atlas is updated (g).

storing the deformation fields from each one of the subjects to the template. The single template is obtained by registering each of the subjects to every other one in the atlas and applying the average deformation field before averaging the resulting warped images, in an iterative approach. When the pipeline is launched, only the transformation between the examined subject and the template will be computed, and the deformation will be combined with the ones already stored. Moreover, a 3-channel registration using the T2-weighted image, gray matter, ventricle probability maps is used, instead of the 2-channel registration implemented in the dHCP pipeline. The comparison between the two approaches is summarised in Figure 2.4.

The probability maps of the different brain tissues are computed using multiple labelled atlases (i.e., ALBERTs atlases in the case of neonates). The atlas labels are transformed and weighted based on their local similarity with respect to the target after registration to merge multiple segmentations into a final weighted structural segmentation, a tissue segmentation and the white and pial boundaries.

2.3.4 Surface extraction

Following segmentation, white-matter and pial surfaces extraction is performed. First, a triangulated surface mesh is fit onto the computed white-matter segmentation boundary. The shape of the mesh is corrected considering possible holes in the segmentation, using the N4 bias-corrected T2-weighted image Schuh et al. (2017). The deformation of the initial surface is driven by a balance of internal and external forces. While the external force seeks to minimise the distance between the mesh vertices and the tissue boundaries, three different internal forces aim to regularise the deformation. They enforce smoothness and avoid self-intersections by introducing a repulsion force and a minimum distance between adjacent vertices and triangles in the mesh. If a movement brings a triangle under the minimum distance from another triangle, the force of its vertices is limited and the movement prevented. Thus, in the first stage, external forces are derived from distances to the tissue segmentation mask, and in the second stage, boundaries are refined using external forces derived

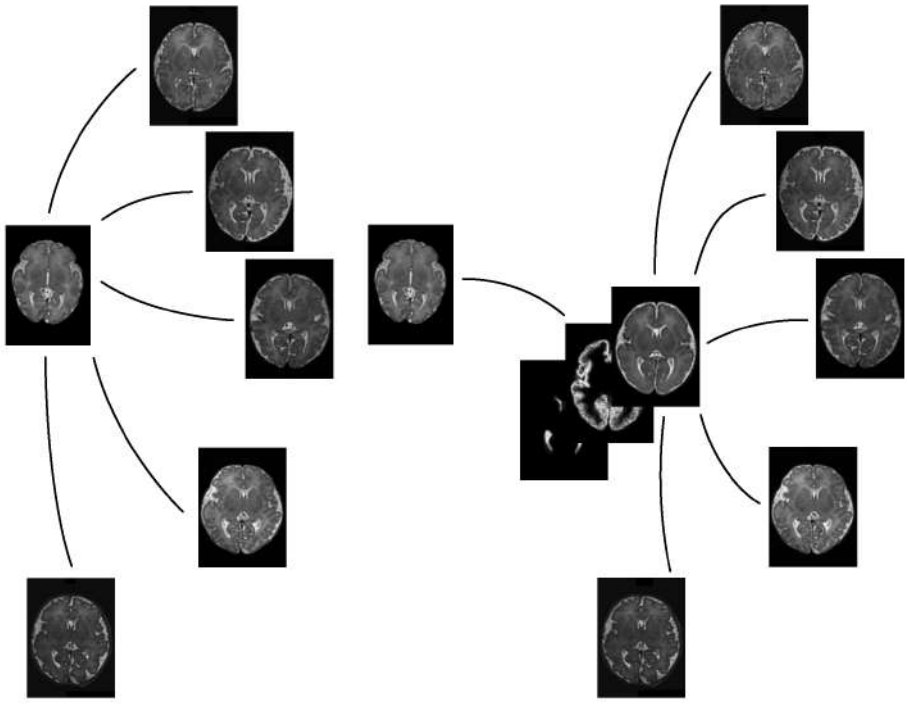

(a) (b)

Figure 2.4: (a) Registration phase as performed in the dHCP pipeline: the subject (left) is registered to each one of the subject composing the multi-subject atlas; (b) Registration phase as performed in the proposed pipeline: the subject is registered to the computed template, and the resulting transformation combined with the previously stored transformations between the template and the subjects composing the multi-subject atlas.

from intensity information. The pial surface is obtained by deforming the white-matter mesh towards the boundary between cortical gray matter (cGM) and CSF, modifying the external force to search for the closest cGM/CSF image edge outside the white-matter mesh. White matter and pial surface extraction allow computing features of the cortical surface, in particular surface curvature, cortical thickness, sulcal depth (i.e. the average convexity or concavity of cortical surface points) and local gyrification index (i.e. a measure of the amount of surface buried in the sulci with respect to the one visible on the surface). More details on the surface extraction process can be found in Makropoulos et al. (2018).

2.4 Results

2.4.1 Temporal template

The fetal template proposed in Gholipour et al. (2017) has been segmented according to the neonatal template presented in Serag et al. (2012a) and originally used in the dHCP pipeline. The neonatal template presented a 7-tissue segmentation, and is used in the dHCP pipeline to have an initial estimation of the tissue segmentation, in particular the grey matter priors, as part of the registration process to obtain the final structural segmentation. Figure 2.5 shows the resulting fetal template segmentation, in which the background label has been added by dilation of the brain mask computed using the BET algorithm.

2.4.2 Multi-subject atlas

A multi-subject fetal atlas has been built selecting 20 subjects and computing on them the same structural segmentation presented in the ALBERTs atlases. In this case, a three-channel registration has been used, including in the registration process the gray matter and ventricle segmentations, alongside the T2-weighted images. Results of the registration are shown in Figure 2.6.

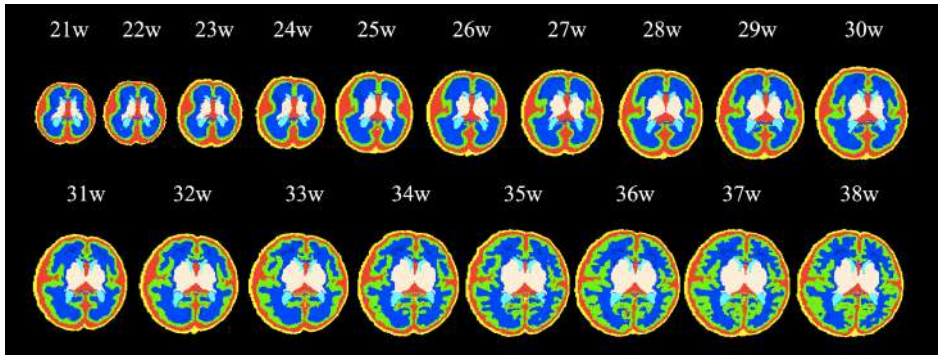

Figure 2.5: Temporal fetal template with the equivalent 7-tissue segmentation.

In order to perform the multi-subject atlas-based segmentation we had to create first a template for each one of the multi-subject atlases (i.e., fetal and neonatal). The templates resulting from this process are shown in Figure 2.7, with the corresponding probability maps.

2.4.3 Segmentation

Using our pipeline, incorporating the new atlases, we are able to accurately segment both early and late-onset subjects, as shown in Figure 2.8.

We can analyse how the implemented tools work for tissue and structural segmentations, for acquisitions at different ages, and show how they compare to the only comparable automatic, end-to-end segmentation tool, the dHCP neonatal pipeline.

The initial tissue estimation depends on the temporal template used. The implementation of the modified fetal temporal template in the pipeline leads to visible improvements in the estimation of the cortical gray matter boundaries and of the ventricles, as shown in Figure 2.9 for a late-onset fetal acquisition segmented both using the dHCP neonatal pipeline and the proposed perinatal pipeline. The estimation of tissue priors is of utmost importance: both gray matter and ventricles priors are used in the multi-subject registration (section 2.3.3), and thus their initial segmentation

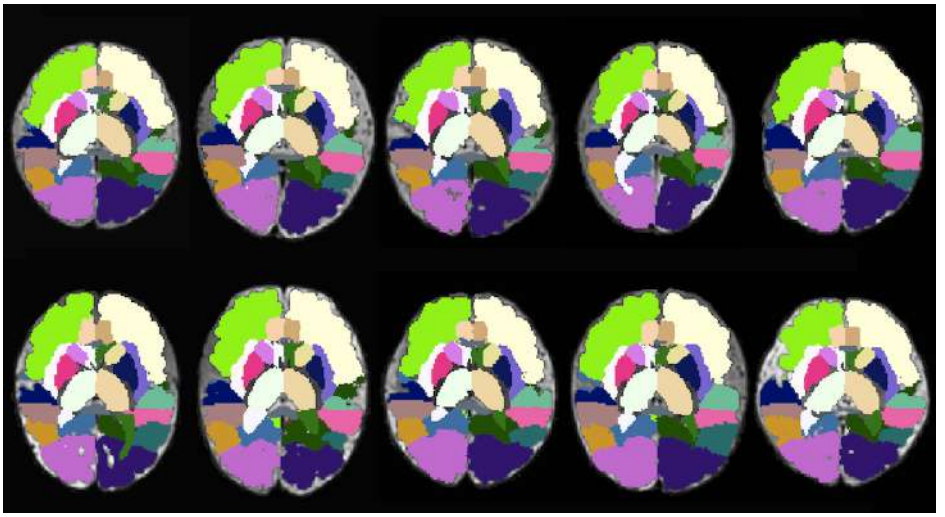

Figure 2.6: Structural segmentation for 10 of the total 20 subjects in the multi-subject atlas.

directly affects the final structural segmentation accuracy.

By using the newly developed fetal templates and modifying the registration method, we can see that the modified pipeline adapts better to early and late-onset fetal acquisitions. Figure 2.10 shows how the use of a fetal structural multi-subject atlas improves the segmentation of the cortical plate, the CSF and the white matter compared to using the nenonatal pipeline.

Quantitative results are given for a subset of 70 fetal acquisitions (Table 2.1). Ground truth for these subjects were provided by manual correction of an expert and compared to the segmentations obtained using the original dHCP neonatal pipeline and our perinatal pipeline. It can be seen that the proposed pipeline improves the segmentation results for cGM, white matter and ventricles.

Moreover, the registration methodology developed allows reducing dramatically the computational load for each segmentation. The time for a single segmentation went from over 3 hours to roughly 15 minutes on an 8-core machine. More importantly, the number of pairwise registrations is

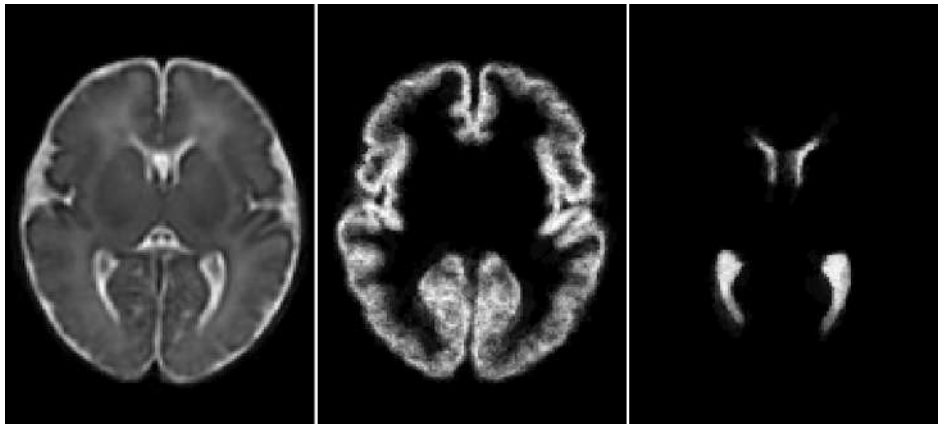

(a)

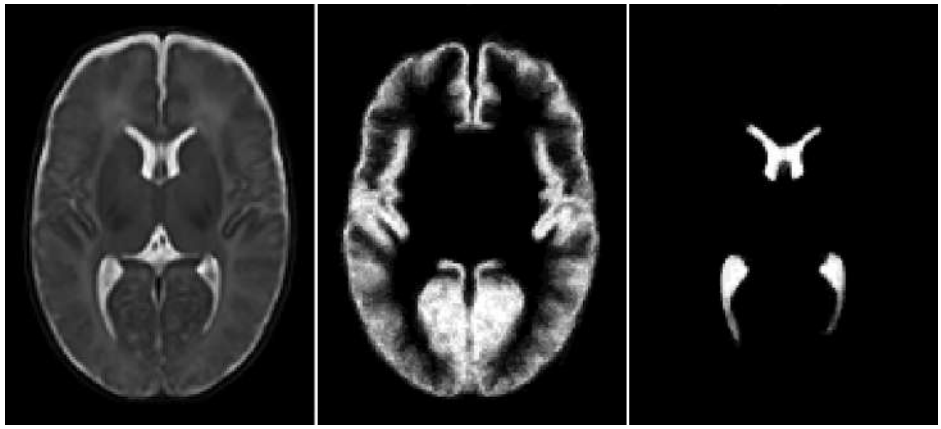

(b)

Figure 2.7: (a) Fetal and (b) neonatal templates obtained from the multi-subject atlases with the cortical gray matter and ventricles probability maps.

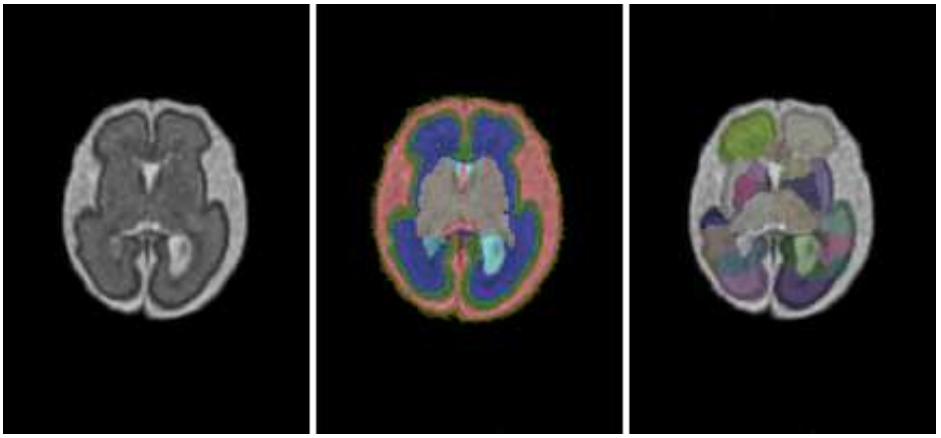

(a)

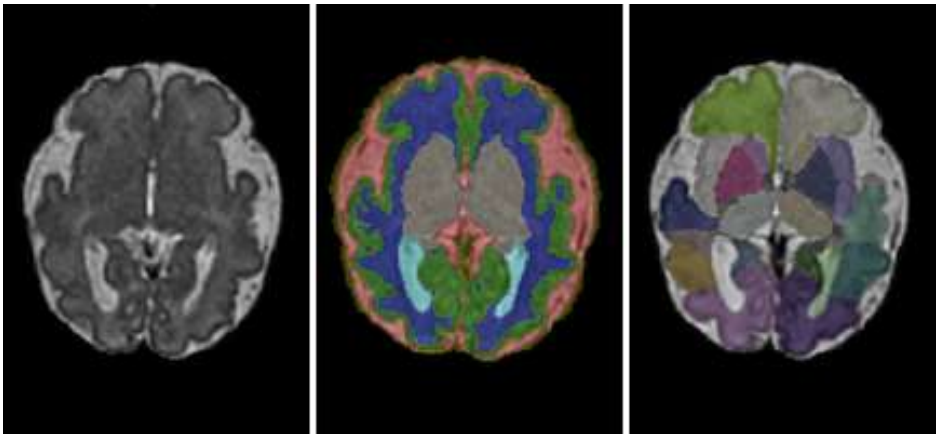

(b)

Figure 2.8: Fetal Segmentation. (a) Early-onset fetal (27 weeks of gestation) T2-weighted image, tissue segmentation and lobular parcellation; (b) Late-onset fetal (32 weeks of gestation) T2-weighted image, tissue segmentation and lobular parcellation.

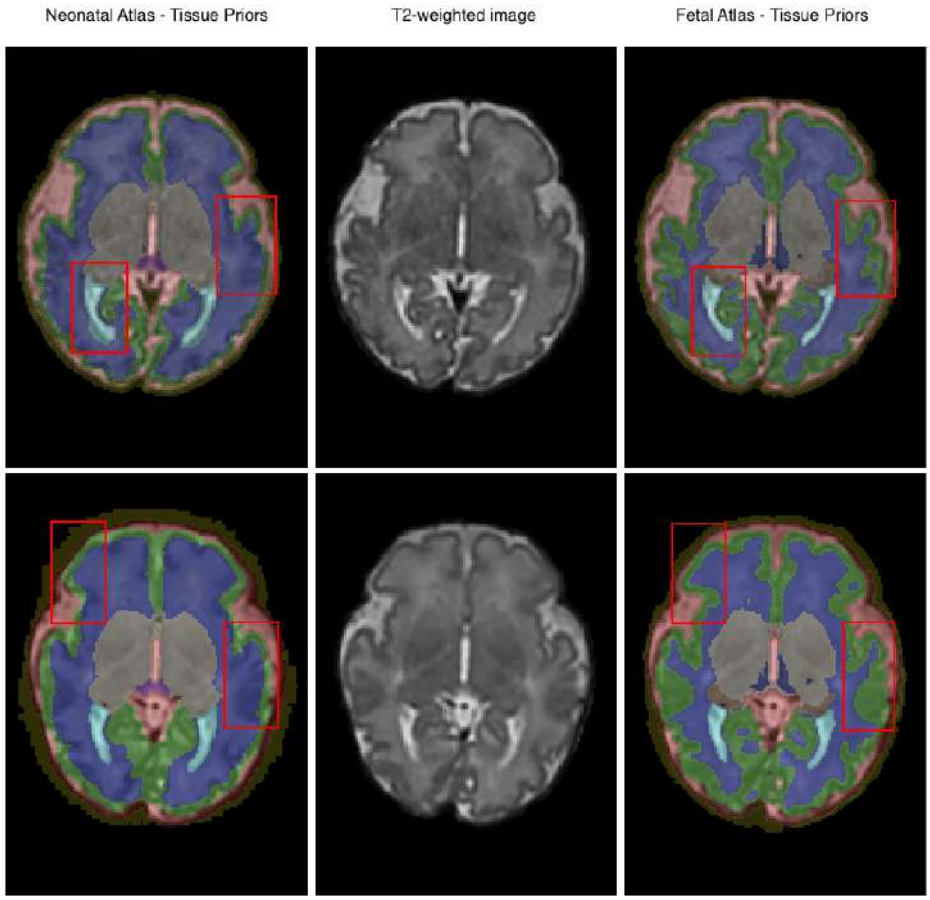

Figure 2.9: Comparison of estimated tissue priors. The figure shows the impact of the use of the enhanced version Gholipour et al. (2017) on the quality of the tissue priors estimation for a late-onset fetus, with respect to the neonatal temporal template.

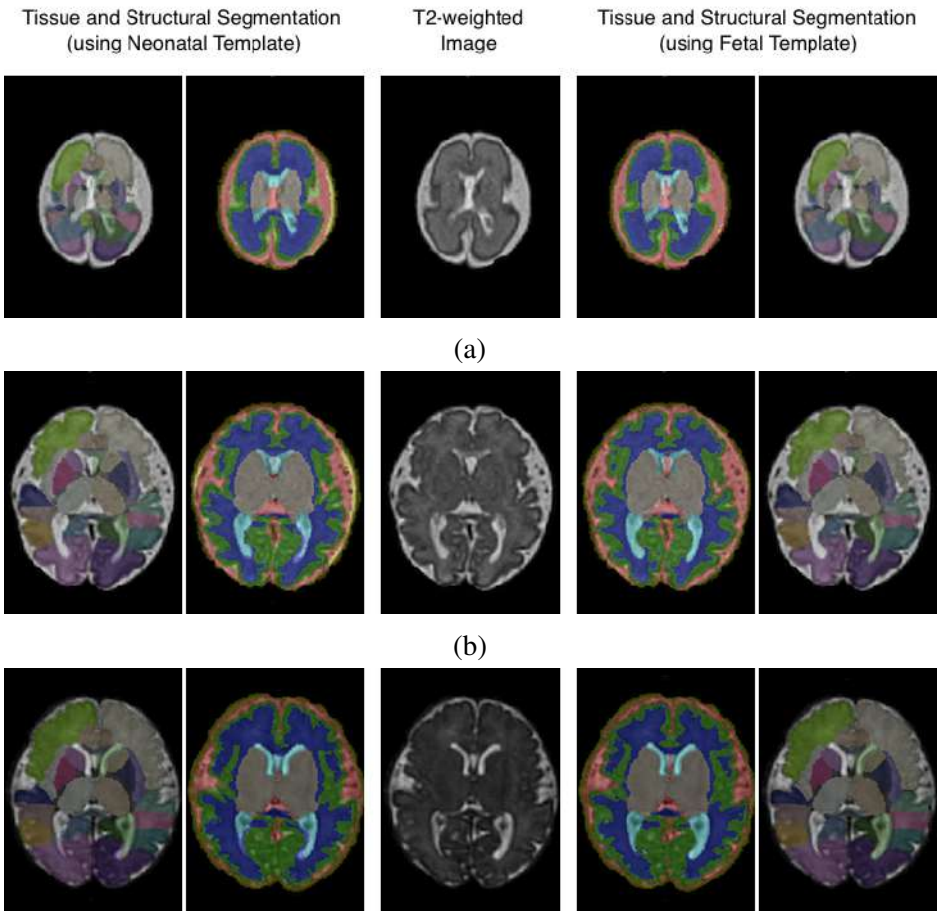

Figure 2.10: Segmentation accuracy qualitative comparison. The figure shows a comparison between the segmentations of 3 fetuses at different gestational ages. (a) Tissue and lobular segmentation at 26.3 weeks of gestation, using a neonatal template and a fetal template respectively. (b) Tissue and lobular segmentation at 33.9 weeks of gestation. (c) Tissue and lobular segmentation at 37.5 weeks of gestation.

Table 2.1: Segmentation accuracy. The table reports the dice coefficient, with respect to the ground truth provided by an expert, of the resulting tissue segmentations using the dHCP pipeline and the proposed perinatal pipeline. The mean dice coefficient (with $\pm$ standard deviation) is reported for each segmented tissue.

Tissue	Neonatal Atlas	Fetal Atlas
CSF	0.79 ± 0.02	0.83 ± 0.04
Cortical Plate	0.76 ± 0.05	0.85 ± 0.03
White Matter	0.85 ± 0.02	0.90 ± 0.02
Ventricles	0.66 ± 0.07	0.73 ± 0.05
Cerebellum	0.89 ± 0.03	0.93 ± 0.02
Brainstem	0.88 ± 0.03	0.92 ± 0.02
Deep Gray Matter	0.90 ± 0.02	0.91 ± 0.01

made constant and equal to one, regardless of the size of the multi-subject atlases.

The three-channel registration has proven to guarantee more accurate results, compared to the simple T2 intensity-based registration and a two-channel registration using the gray matter probability maps. Tissue segmentation can be derived from the structural segmentation and compared to the ground truth provided by an expert. Dice coefficient was computed to quantify the overlap with the ground truth segmentation. As 2.2, segmentation improves for the internal structures (e.g.: ventricles, deep gray matter).

2.4.4 Surface extraction

Extraction of the cortical surface from segmentation allows analyzing differences in shape, and thus gives more information on the brain development. Reconstruction can be applied to fetal and neonatal subjects using the enhanced pipeline. Figure 2.11 shows the reconstruction for an early stage fetus, for a late stage fetus and a neonate.

Table 2.2: Registration method comparison. The table reports the dice coefficient, with respect to the ground truth provided by an expert, of the resulting tissue segmentations using one, two and three channels for the registration respectively. The mean dice coefficient (with $\pm$ standard deviation) is reported for each tissue segmented.

Tissue	T2-based	2-channel	3-channel
CSF	0.83 ± 0.02	0.85 ± 0.01	0.83 ± 0.04
Cortical Plate	0.75 ± 0.05	0.83 ± 0.03	0.85 ± 0.03
White Matter	0.85 ± 0.02	0.89 ± 0.02	0.90 ± 0.02
Ventricles	0.65 ± 0.07	0.68 ± 0.05	0.73 ± 0.05
Cerebellum	0.92 ± 0.03	0.91 ± 0.03	0.93 ± 0.02
Brainstem	0.91 ± 0.03	0.88 ± 0.03	0.92 ± 0.02
Deep Gray Matter	0.90 ± 0.02	0.90 ± 0.02	0.91 ± 0.01

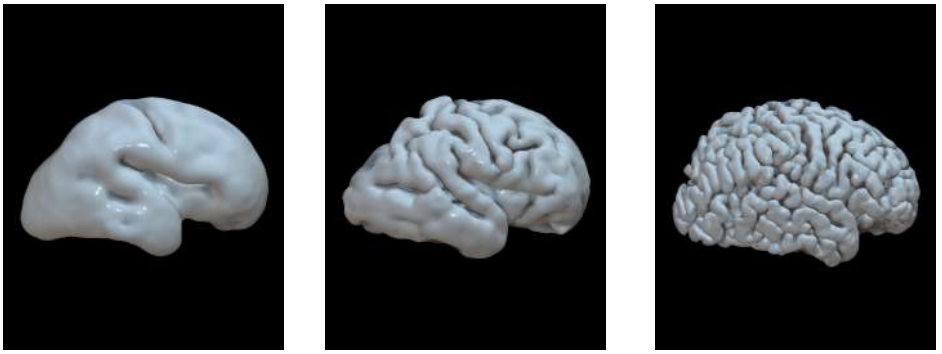

(a) (b) (c)

Figure 2.11: Extracted surfaces for fetuses and neonates. The figure shows the increasing complexity and convoluted shape of the cortex for (a) an early-onset fetus (26.7 weeks of gestation), (b) a late-onset fetus (32.4 weeks of gestation) and (c) a neonate (44.1 weeks of gestation).

2.4.5 Feature Extraction

After cortical surface extraction, shape features of interest for the brain development assessment can be computed using the calculated meshes. In particular, we focus on curvature, local gyrification index (LGI), sulcal depth and thickness.

Mean Curvature Mean curvature is estimated from the average of the principal curvatures of the white matter surface. The principal curvatures represent the minimum and maximum bending of a regular surface at each given point. Mean curvature tends to increase while the cortex grows and gets more convoluted, whereas at an early stage in the development, the less complex shape of the cortical plate involves a lower mean curvature, as it can be seen in Figure 2.12a.

Local Gyrification Index Local gyrification index is computed as the ratio between an area taken on the cortical surface of the brain and the area covered by the same points on the inflated surface Lyu et al. (2018). The inflation process moves outwards the points in the sulci and brings in the points on the gyral crowns - preserving distance between neighboring vertices - until a certain smoothness is reached. It can be seen on the average fetal brain as LGI tends to zero where the surface is flat, while it has higher values in the depth of the main sulci (Figure 2.12b).

Sulcal Depth Sulcal depth represents the average convexity or concavity of cortical surface points. Being directly related to the presence of sulci on the cortex, it is higher in the more convoluted parts of the brain (Figure 2.12c) and it naturally increases while the brain grows, whereas for a fetal brain has lower values.

Cortical Thickness Cortical thickness is defined as the average distance between two measures: 1) the Euclidean distance from the white surface to the closest vertex in the pial surface; 2) the Euclidean distance from the pial surface to the closest vertex in the white surface.

Thickness is higher at early stage, as the cortex becomes thinner to be able to bend on itself while it grows.

2.5 Discussion

This paper presents a new pipeline, built upon the structure of the dHCP neonatal pipeline Makropoulos et al. (2018), for the structural segmentation and cortical surface extraction of fetal and neonatal brain MRI. The modification and adaptation of an existing fetal temporal template, and the creation of a new multi-subject fetal atlas are also reported. This pipeline allows for a consistent and coherent fetal and neonatal segmentation in the same framework, for the analysis of perinatal data and thus with potential application to longitudinally acquired data. Moreover, a new registration approach has been proposed and, consequently, the segmentation has been made more robust by adding a new channel (i.e. the ventricle probability maps) to the multi-subject atlas registration.
The modifications applied to the registration process lead to an improved neonatal segmentation compared to the dHCP neonatal pipeline. When compared on a fetal dataset, results show how the segmentation accuracy was enhanced by using fetal templates for all the main tissues: considering both the external cortical surface and the internal shape of the ventricles in the transformation leads to a more accurate overall registration.
Moreover, for both neonatal and fetal acquisitions, the proposed registration approach leads to a reduced computational load, and it makes the process scalable. This leads to the possibility of increasing the number of the subjects in both the fetal and neonatal atlases, enhancing their validity without affecting the computational load of the pipeline.
Finally, the surface extraction process has proven to be efficient for fetal images, based on an expert qualitative analysis, faithfully reporting the convoluted shape of the cortical surface resulting from the segmentation in the 3D regularised mesh computation. The possibility of computing a structural and regional segmentation for both fetal and neonatal images, and to extract the cortical surfaces, opens a variety of possible analysis to

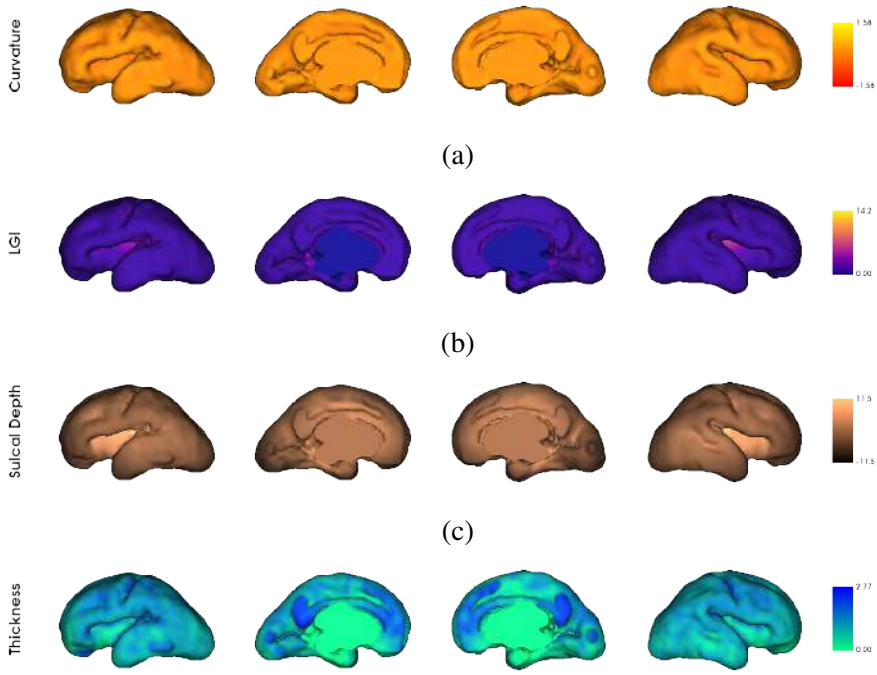

Figure 2.12: Cortical morphological features of a fetal subject. The figure shows the extracted cortical feature for a fetus, in particular (a) mean curvature, (b) local gyrification index (LGI), (c) sulcal depth and (d) thickness.

be carried out in the future.
Future works will focus on further improving and enhancing the performance of the pipeline, with the possible implementation of deep learning-based approaches for registration, which would further reduce the computational load and shorten the segmentation process. It would also be possible to increase the size of the used multi-subject atlases, including also pathological anatomies and widening the temporal window covered by the subjects to enhance the range of application of the pipeline. Furthermore, of particular interest from a clinical perspective could be the analysis of local cortical features in longitudinally acquired data, and their relationship with other brain features and diseases.

Chapter 3

A LONGITUDINAL STUDY OF THE RELATIONSHIP BETWEEN VENTRICULOMEGALY AND CORTICAL FOLDING IN FETUSES AND NEONATES

Abstract – The impact of ventriculomegaly (VM) on cortical development and brain functionality has been extensively investigated in the literature. VM has been found to be related to higher risks of attention-deficit and hyperactivity disorders, and cognitive, language, and behavior deficits. Some works have shown a relationship between VM and cortical overgrowth as well as reduced cortical folding in both fetuses and neonates. In this work, using a longitudinal dataset of 30 subjects (15 healthy controls and 15 subjects diagnosed with VM) with structural MRI acquired in and ex utero for each subject, we investigated the impact of fetal VM on cortical development from a longitudinal perspective, from fetal to neonatal stage. Particularly, we studied the relationship of ventricular enlargement with both volumetric features and a multifaceted set of cortical folding measures, namely: local gyrification, sulcal depth, curvature and cortical thickness. Our results show significant effects of VM on both volumetric and morphometric descriptors of cortical development in specific areas of the brain including the occipital, parietal and frontal lobes. These findings are in alignment with the literature, confirming the presence of longitudinally significant cortical overgrowth and delayed cortical folding in VM subjects from the fetal to neonatal stage.

This chapter is adapted from:
A. Urru A., Benkarim O. M., Hahner N., Piella G., Eixarch E., González Ballester M. A., A Longitudinal Study of the Relationship between Ventriculomegaly and Cortical Folding in Fetuses and Neonates. *Submitted to Neuroimage: Clinical*,, 2022.

3.1 Introduction

In the human brain, gyri are convex formations surrounded by sulci, which represent concave bendings of the cortical plate. Deeper, larger sulci are called fissures, and they divide the different lobes and the two brain hemispheres. Combinations of gyri and sulci allow the brain to have a very large cortical surface, and thus a large number of neuronal connections, without the need for a proportional enlargement of the whole brain. Even though not completely understood yet, the convolutional patterns of the cerebral cortex are closely related to its architectural and functional specialization Fernández et al. (2016); Toro and Burnod (2005). Moreover, some studies have also shown a relationship between the convolutional pattern of the cortical plate and its cytoarchitecture Fischl et al. (2008). Hence, the understanding and modeling of these patterns and their regulating mechanisms have drawn increasing attention in research. What is clear from the studies on cortical development is that the formation of primary sulci follows consistent patterns across subjects (e.g., the Sylvian fissure) Armstrong et al. (1995); Chi et al. (1977); Griffiths et al. (2010), whereas the formation of the smaller, more superficial secondary and tertiary sulci is governed by more irregular patterns. Although at the end of gestation most major sulci and gyri are well established, tertiary sulci continue to develop from fetal to neonatal stage Voorhies et al. (2021).

Understanding the mechanisms underlying cortical development may help improve both diagnosis and treatments in case of abnormal growth. An abnormal development of the cortex, in fact, could be the outcome of a pathological condition, such as ventriculomegaly (VM) Benkarim et al. (2020, 2018a, 2017); Kyriakopoulou et al. (2014); Scott et al. (2013), which may be related to disorders such as schizophrenia, autism and attention deficit in adults Jou et al. (2005); Landrieu et al. (1998); Nordahl et al. (2007); Sallet et al. (2003); Wolosin et al. (2009). VM is one of the most common anomalies in fetuses and neonates, with an incidence of around 1% among fetuses Huisman et al. (2012); Salomon et al. (2007). VM can affect one or both ventricles, and it is generally defined by an atrial diameter larger than 10 mm at any fetal stage (from 14 gestational weeks onwards).

Abnormal ventricular development has been shown to be associated with cortical overgrowth in fetuses Benkarim et al. (2018b); Kyriakopoulou et al. (2014) and with dysfunctional behaviours in neonates Hahner et al. (2019). Still, the full extent in which VM may influence postnatal neurodevelopment remains largely unclear due to the lack of postnatal and long-term follow-up studies. When VM is diagnosed in utero, postnatal prognosis depends on the presence of other abnormalities and the severity of the ventricular dilation, both contributing to the worsening of outcomes. In this work, we focus on isolated non-severe VM (INSVM), which is diagnosed by an atrial diameter between 10 and 15 mm, and in the absence of other abnormalities. INSVM can be further classified into mild (10 to 12 mm) or moderate (12 to 15 mm). Although most fetuses diagnosed with INSVM are unlikely to have long-term neurodevelopmental deficits Griffiths et al. (2010); Melchiorre et al. (2009), there are a few that will have unfavorable outcomes Gómez-Arriaga et al. (2012); Leitner et al. (2009); Sadan et al. (2007). Thus, elucidating the factors that might influence the postnatal outcome of fetuses diagnosed with INSVM is critical for clinical counseling and decision-making.

Magnetic resonance imaging (MRI) is increasingly being adopted for monitoring and quantifying brain development. For VM, particularly, MRI is indicated for both in and ex utero diagnosis Rutherford (2002). Moreover, several works leveraged 3D MRI to model and analyze fetal brain development in healthy cohorts Habas et al. (2010); Kuklisova-Murgasova et al. (2011); Serag et al. (2012b) as well as in non-healthy subjects de Dumast et al. (2020); Payette et al. (2021, 2020). While the former build models to characterize normative brain development in fetuses and neonates, neuroimaging of diseased brains allows finding patterns of disease-specific deviations from the normative neurodevelopment that can be potentially used as biomarkers to accurately identify such diseases. For VM, there are several studies inspecting the relationship between ventricular enlargement and cortical development Benkarim et al. (2020, 2018a); Kyriakopoulou et al. (2014); Scott et al. (2013), reporting notably marked associations of VM with both cortical volume and the degree of cortical folding. Nonetheless, these studies were conducted in cross-

sectional datasets composed of only fetuses or neonates, which prevents us from having a clear picture of the longitudinal changes in cortical development of fetuses diagnosed with VM.

Here, using a longitudinal dataset of 30 subjects (15 healthy controls and 15 subjects diagnosed with INSVM) with structural MRI acquired in and ex utero for each subject, we conducted, to the best of our knowledge, the first longitudinal study investigating the impact of VM on cortical development ranging from fetal to neonatal stage. Particularly, we examined the relationship of ventricular enlargement with both volumetric features and a multifaceted set of cortical folding measures, namely: local gyrification, sulcal depth, curvature and cortical thickness. Moreover, both global and local differences between subjects with VM and healthy controls were analysed. Our findings highlighted a delayed cortical development taking place from fetal to neonatal stage, simultaneously represented by lower gyrification and higher cortical thickness, especially in the frontal, occipital and parietal lobes throughout the investigated temporal window. Our findings also confirm the presence of longitudinally significant cortical overgrowth reported in previous works Kyriakopoulou et al. (2014), linking it to an abnormal development of the cortex in terms of thickness and gyrification.

3.2 Materials and Methods

3.2.1 Dataset

The dataset used in this study was composed by the MRI acquisitions from 30 subjects, divided in 15 healthy controls and 15 subjects with INSVM diagnosed based on the ventricular diameter at ultrasound. In particular, the age range at the time of scan was 26.2 to 33.7 weeks post-menstrual age (PMA) for fetal acquisitions, while neonatal images had an age range between 41.29 to 47.57 weeks PMA. The whole dataset was thus composed by a total of 60 images, two for each subject. Demographics details on the dataset are presented in 3.1.

3.2.2 MRI Acquisition

Fetuses

For in utero acquisitions, T2-weighted MRI was performed on a 1.5-T scanner (SIEMENS MAGNETOM Aera syngo MR D13; Munich, Germany) with a 8-channel body coil. All images were acquired without sedation and following the American College of Radiology guidelines for pregnancy and lactation. Half Fourier acquisition single shot turbo spin echo (HASTE) sequences were used with the following parameters: repetition time (TR) = 1500 ms, echo time (TE) = 82 ms, number of averaging = 1, slice thickness = 2.5 mm, field of view (FOV) = 280 $\times$ 280 mm, and voxel size = 0.5 $\times$ 0.5 $\times$ 2.5 mm. For each subject, multiple orthogonal acquisitions were performed: 4 axial, 2 coronal and 2 sagittal stacks.

Neonates

Neonatal images were acquired during natural sleep using a TIM TRIO 3.0 T whole body MR scanner (Siemens, Germany). T2-weighted images were obtained with the following parameters: 2-mm slice thickness with 2 mm interslice gap, in-plane acquisition matrix of 256 $\times$ 256, FOV = 160 $\times$ 241 mm, which resulted in a voxel dimension of 0.625 $\times$ 0.625 $\times$ 2 mm, TR = 5980 ms and TE = 91 ms. All acquired MRI scans were visually inspected for apparent or aberrant artifacts and brain anomalies and subjects excluded accordingly. Table 3.1 shows the demographics of the complete dataset.

3.2.3 Processing pipeline

Both fetal and neonatal brain images were segmented using the automatic segmentation pipeline described in Urru et al. (2022). Briefly, the pipeline uses an atlas-based label fusion segmentation approach based on atlases with a similar age to that of the target image. The pipeline produced tissue-level and regional segmentations for each subject. Once the segmentations of the main tissues were obtained, inner and outer cortical surfaces were

Table 3.1: Demographics. The table reports the number of participants in each group (i.e., healthy controls and VM subjects), proportion of males and females (M/F) in each group, mean ($\pm$ standard deviation) age and ventricular volume (VV) for each group and timepoint (i.e., fetal and neonatal). Group differences were assessed using t-test for continuous variables (i.e., age, ventricular volume) and Chi-squared test for binary variables (i.e., sex).

	N	Sex (M/F)	Age (weeks)		VV (cm^3)	
			Fetal	Neonatal	Fetal	Neonatal
Control	15	9/6	29.6 ± 3.1	43.6 ± 1.4	3.74 ± 1.16	5.18 ± 1.00
VM	15	13/2	28.7 ± 2.3	43.6 ± 1.7	9.87 ± 4.04	12.86 ± 5.71
p-value		0.082	0.174	0.458	<0.001	<0.001

extracted. The following cortical features for each subject were computed: mean curvature, cortical thickness, sulcal depth, and local gyrification index (LGI). The processing pipeline, from image acquisition to features extraction, is shown in Figure 3.1.

Segmentation and Surface Extraction

For fetuses, 3D motion-corrected reconstructions were obtained from the acquired 8 stacks of thick 2D slices. Brain location in each 2D slice was carried out in an automatic manner using the approach proposed by Salehi et al. (2018), followed by high-resolution 3D volume reconstruction using the method presented in Ebner et al. (2019, 2018b). Segmentation proceeded with a brain-extraction step, implemented using the Brain Extraction Tool (BET) Smith (2002) to remove the remaining extra-brain tissue (e.g., parts of the skull) in both fetuses and neonates. Once the brain was extracted, it was rigidly registered to the corresponding template and intensity inhomogeneity corrected.

Subsequently, the segmentation was performed using an Expectation-Maximization algorithm. Each subject was initially registered, using image intensity, to a temporal template and a first tissue segmentation estimation

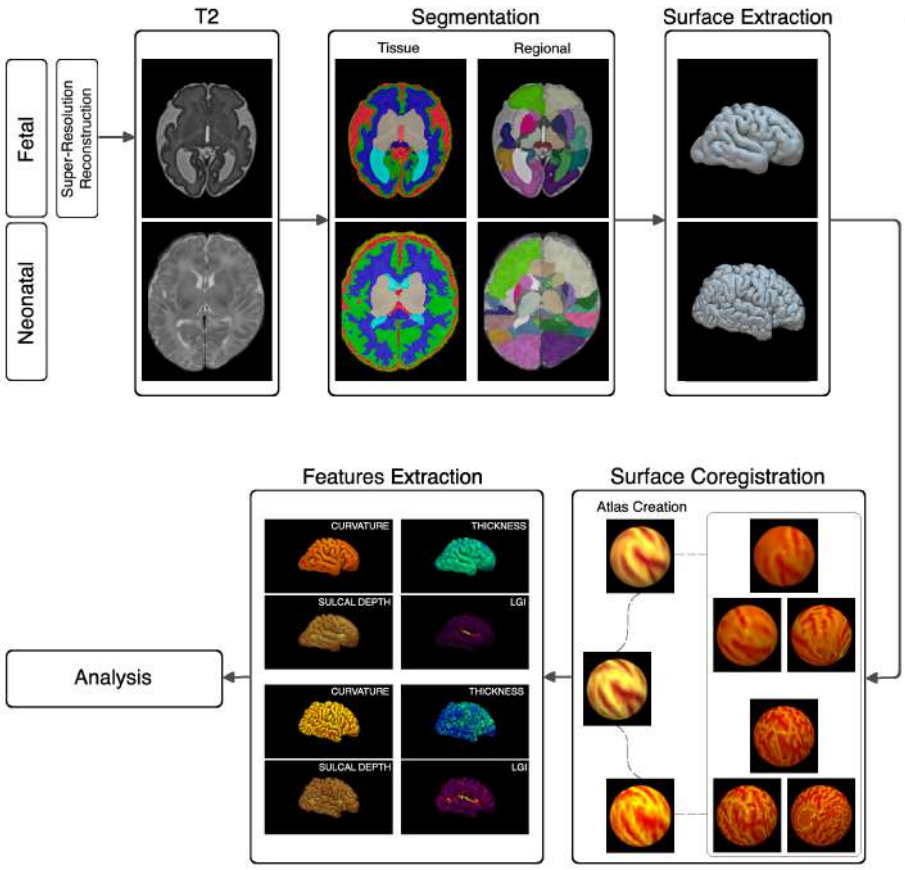

Figure 3.1: Processing pipeline. After performing a high-resolution reconstruction for fetal images, we generated tissue and regional segmentations. Next, inner and outer cortical surfaces were generated and cortical features (i.e., mean curvature, sulcal depth, thickness and local gyrification index) were computed. Spherical Demons was then used to establish vertex-wise correspondences between individual surfaces within the same timepoint (i.e., between fetuses and between neonates), followed by atlas generation for fetuses and neonates, and the alignment between these atlases establish vertex-wise correspondence between fetal and neonatal surfaces.

was computed accordingly. In a second step, a 3-channel registration (using the T2-weighted image, gray matter and ventricle probability maps) to a multisubject atlas was used to compute a regional parcellation and subsequently refine the tissue segmentation in the previous step.

Next, white-matter and pial surfaces were extracted. For each subject, a triangulated surface mesh was fit onto the computed white-matter segmentation boundary. The pial surface was obtained by deforming the white-matter mesh towards the boundary between cortical gray matter (cGM) and cerebrospinal fluid (CSF), looking for the closest cGM/CSF image edge outside the white-matter mesh, and adding a regularization term to smoothen the resulting mesh. The full description and applications of the processing pipeline can be found in Urru et al. (2022).

Atlas Creation

The cortical surface meshes extracted from the previous step were not in vertex-wise correspondence. To standardize the topology and establish correspondence between vertices, our cortical surfaces were registered to a common reference frame using Spherical Demons Yeo et al. (2010). This algorithm performs the registration of two surfaces based on their spherical projections with geometric features at each vertex (e.g., mean curvature). In this case, given the considerable differences between fetal and neonatal cortices, Spherical Demons was performed separately for each hemisphere and timepoint. This procedure resulted in a total of four spherical atlases, each one representing a hemisphere and timepoint. Subsequently, each mesh was regularized based on the atlas size and topology by means of the iterative closest point (ICP) algorithm Besl and McKay (1992). These steps brought the spherical projections in correspondence, for each timepoint, and the cortical meshes were remeshed accordingly.

In order to perform a longitudinal vertex-wise analysis, we furthermore need both fetal and neonatal surfaces to be registered to the same reference frame. Although the cortex is substantially more convoluted in neonates than in fetuses, there are prominent cortical landmarks such as the primary sulci and gyri that are formed as early as the 14 gestational week and can

be identified at both timepoints (e.g., central and lateral sulci). These are most likely to drive the coregistration procedure between the fetal and neonatal atlases. Spherical Demons was then applied again to the two sets of atlases previously computed and two atlases (one for each hemisphere) were finally obtained, which brought in correspondence all the subjects at both timepoints.

Characterization of Cortical Folding

Once the cortical surfaces were extracted, we computed four different geometric features to characterize cortical folding, namely: mean curvature, local gyrification index, sulcal depth and thickness.

Mean Curvature Mean curvature is estimated from the average of the principal curvatures of the inner surface. The principal curvatures represent the minimum and maximum bending of a regular surface at each given point King et al. (2016). This descriptor tends to increase while the cortex grows and gets more convoluted, whereas at an early stage in the development, the less complex shape of the cortical plate involves a lower mean curvature.

Local Gyrification Index This descriptor is computed as the ratio between an area taken on the cortical surface of the brain and the area covered by the same points on the inflated surface. The inflation process moves outwards the points in the sulci and brings in the points on the gyral crowns - preserving distance between neighboring vertices - until a certain smoothness is reached Lyu et al. (2018). It can be seen on the average fetal brain that LGI tends to zero where the surface is flat, while it provides the highest values in the deepest parts of the main sulci.

Sulcal Depth Sulcal depth represents the distance of a vertex on the convoluted cortical surface from the corresponding vertex on the convex hull obtained by inflating the cortical surface Yun et al. (2013). Being

related to the degree of gyrification of the cortex, sulcal depth increases with brain development.

Thickness Cortical thickness is defined as the average distance between two measures: 1) the Euclidean distance from the inner surface to the closest vertex in the outer (i.e., pial) surface; and 2) the Euclidean distance from the pial surface to the closest vertex in the inner surface. Cortical thickness is highest in early development, and it gradually decreases as the cortex becomes thinner to be able to bend on itself while it grows Amlien et al. (2016); Brown et al. (2012); Sowell et al. (2004).

Global Analysis

In our first analysis, we investigated global group differences based on the volumes of the main tissues as well as on cortex-wide folding features. Ventricles, cortical grey matter, white matter and supratentorial volumes were all computed based on the previously generated segmentations. For the morphometric features, they were corrected for age and sex effects, and the distributions of the two groups were log-transformed to normalize them. A Student t-test was then used to assess the differences between the groups for every cortical folding feature and for each timepoint. Results from this initial analysis are presented in section 3.3.1.

Volumetric Analysis

Subsequently, we went on analyzing lobular volumes and inspecting between-group differences for each timepoint as well as longitudinally. For this analysis, we used the regional parcellations, which divided the cortex in six different regions: cingulate gyrus, insula, frontal, occipital, parietal and temporal areas. We analyzed the differences by fitting group-level growth trajectories for each of them. Moreover, we investigated the percentage mean difference for each timepoint separately, after correcting for the effects of age and sex. Finally, we also analyzed local volume differences from a longitudinal perspective, using a mixed-effects

model Raudenbush and Bryk (2002) to predict the volume of each of the aforementioned cortical areas. A mixed-effects model combines fixed and random effects, and it allows to model independent multiple acquisitions of the same subjects through time. In our case, we acquired two images for each subject, at fetal and neonatal stage. We tested the effect of diagnosis on lobular volumes, with age and sex as fixed-effect covariates and the multiple acquisitions as a random effect:

$$V_{lobe} = \beta_0 + \beta_1 GA + \beta_2 S + \beta_3 DG + \alpha ID, \tag{3.1}$$

where V_{lobe} represents the predicted lobular volume, GA is the age in weeks, S denotes the sex of the subjects (0 for female, 1 for male), DG stands for diagnosis (0 for control, 1 for VM), while ID is a unique identifier for each subject. Results of the analysis are presented in section 3.3.2.

Morphometric Analysis

Finally, we conducted a vertex-wise morphometric analysis to assess the relationship between ventricular enlargement and cortical folding, which was characterized using 4 different descriptors as described above. The analysis was carried out using a mixed-effects model to predict the cortical folding features at each vertex. In particular, here we use a more complex model, adding some interaction between covariates to establish the effect of diagnosis (i.e., the presence of abnormal ventricular development) on cortical folding:

$$F_i = \beta_0 + \beta_1 GA + \beta_2 S + \beta_3 DG + \beta_4 GA * VV + \alpha ID, \tag{3.2}$$

where F_i represents the modeled cortical feature, GA is the age in weeks, S the sex of the subjects (0 for female, 1 for male), DG the diagnosis (0 for control, 1 for VM), VV represents ventricular volume, and ID is a unique identifier for each subject. As we can see in this model, we included a quadratic effect of age and interactions between age and ventricular volume. Results of the analysis are presented in section 3.3.3.

Furthermore, we assessed the relationship between the map of group-wise difference in local gyrification index and those of the remaining cortical folding descriptors (i.e., group-wise differences in mean curvature, sulcal depth, and cortical thickness) using Spearman's correlation. For this analysis, we accounted for spatial autocorrelations using nonparametric permutation tests (i.e., spin tests) Alexander-Bloch et al. (2018).

3.3 Results

3.3.1 Global Analysis

In the first analysis we focused on global differences in brain development. Specifically, we studied ventricular and cortical volumes and the previously mentioned morphometric features averaged throughout the whole cortex, to quantify differences between controls and ventriculomegaly patients at the two investigated timepoints.

Figure 3.2 shows the difference between controls and VM subjects in terms of ventricular and cortical volume respectively, including both single-subject and group-level growth trajectories. Regarding morphometric features, the average values across the cortical surface were computed, corrected for the effects of age and sex and log-transformed to normalize the distributions in each cohort, before applying a Student t-test at each timepoint, for each feature, between the two groups.

This initial analysis showed potentially significant differences both in volumetric and morphometric features between the groups. As expected, we found a remarkable and time-consistent difference in terms of ventricular volumes between the groups, whereas only a slight difference was revealed in terms of cortical volume. In particular, from early to late-onset fetuses, we see a steeper growth in cortical volume in VM subjects with respect to controls. With regard to morphometric features, we found significant differences in terms of curvature and local gyrification index only in neonates. Moreover, we found a reduction in gyrification-related features in VM subjects across the investigated timepoints, with higher values of cortical thickness in VM subjects at neonatal stage. This can be related to

cortical volume growth trajectories as a thicker, less gyrified cortex could lead to a higher total volume.

This analysis provides a global depiction of the differences in cortical development between VM subjects and healthy controls. In subsequent sections, we carried out more fine-grained analyses focusing on lobular volumes and vertex-wise morphometry.

3.3.2 Volumetric Analysis

In this analysis we studied differences in lobular volumes between the cohorts. An analysis of the mean differences between the cohorts highlighted the lobes with the highest differences in volume between the groups at the two timepoints. Finally, a mixed-effects model was applied to predict each lobe volume and the corresponding t-value computed and projected on the average neonatal brain.

Figure 3.3 shows differences in terms of volumetric development in the different lobes of the cortex. We also computed mean percentage differences between the cohorts for each timepoint. Before doing so, volumes were corrected for the effects of age and sex. From a longitudinal point of view, we used a mixed-effects model to predict each lobular volume and find the regions in which volume significantly differed between VM subjects and controls.

Results showed a consistent pattern in terms of volumetric growth in the insula, but also in the frontal, occipital and parietal lobes, with a steeper growth from early to late-onset observed in VM subjects with respect to controls. In terms of percentage difference in volume at the two investigated timepoints, we found particularly high differences in the cingulate gyrus area, especially at fetal stage, and also in the frontal, occipital and parietal lobes. From a longitudinal point of view, results showed increased volumes throughout the whole cortex in VM subjects with the most significant differences between the groups located in the cingulate gyrus and in the frontal, occipital, parietal lobes. These results are in alignment with previous findings Kyriakopoulou et al. (2014) showing a cortical overgrowth in VM subjects, and extend their validity longitudinally,

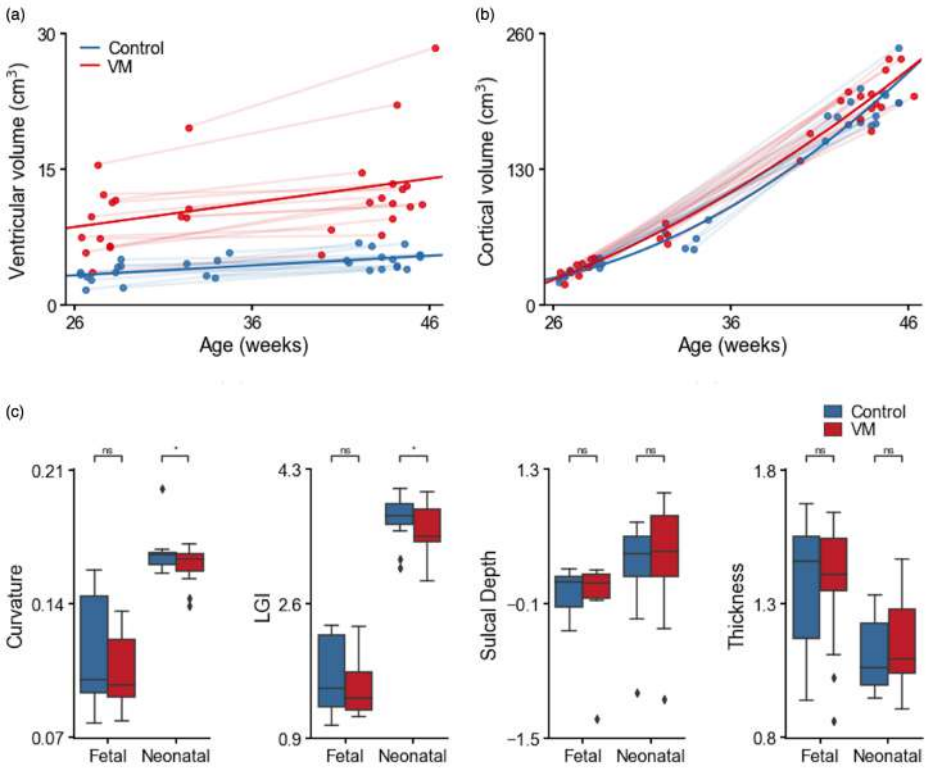

Figure 3.2: Global differences in volumetric and morphometric developmental trajectories. (a) Total ventricular volume (VV) growth trajectories for healthy controls and VM subjects (from fetal to neonatal stage). (b) Cortical area growth trajectories for healthy controls and VM subjects. Group-level and individual trajectories are displayed using solid and dashed lines respectively. (c) Group-wise distributions of mean curvature, cortical thickness, local gyrification index (LGI), and sulcal depth at both fetal and neonatal stages. Boxes denote the interquartile range (IQR) between the first and third quartiles, and the line inside denotes the median. Whiskers extend to points that lie within 1.5 IQRs of the lower and upper quartiles, and the black diamonds denote outliers. Significant differences between groups are denoted using an asterisk (*).

from fetal to neonatal stage.

3.3.3 Morphometric analysis

Finally, we conducted a vertex-wise analysis to assess group-wise morphometric differences. We used vertex-wise mixed-effects models including different covariates: age, sex, diagnosis and ventricular volume (VV) as fixed effects, and each subject's ID as random effect. This analysis produced cortical t-maps showing group-wise differences for each morphometric descriptor across the whole cortex. Figure 3.4 displays the t-maps corresponding to mean curvature, sulcal depth, LGI, and cortical thinckness, as well as clusters with significant differences in LGI and thickness.

Results showed negative t-values across the whole cortex for curvature and local gyrification index, whereas for thickness we found positive t-values, except for some small clusters. Sulcal depth presented more diversified group-wise differences. We further assessed the correlations between the t-map of LGI and t-maps of remaining cortical folding features using spin tests with 1000 permutations to account for spatial autocorrelation Alexander-Bloch et al. (2018), finding a particularly significant negative correlation between LGI and thickness. LGI presented significantly lower values in VM subjects in clusters within the frontal, occipital and temporal lobes. Cortical thickness, on the other hand, presented significant clusters in the frontal, occipital and parietal areas, where thickness was considerably higher in VM subjects with respect to healthy controls.

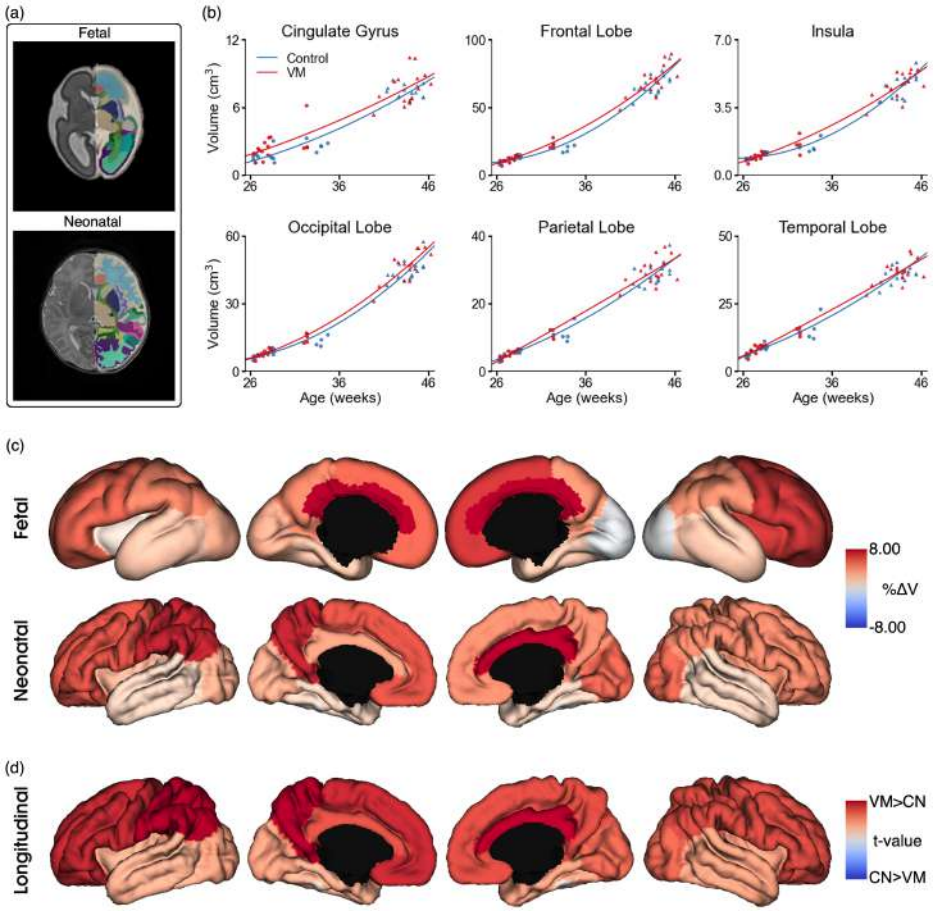

Figure 3.3: Volumetric Analysis. (a) Examples of regional parcellation shown for the same subject at both fetal and neonatal stages. (b) Lobular volume growth trajectories for healthy controls and VM subjects. (c) Percentage differences in volume between the groups are displayed on the fetal and neonatal average brains respectively. (d) T-values computed using a mixed-effects model to predict each lobe's volume.

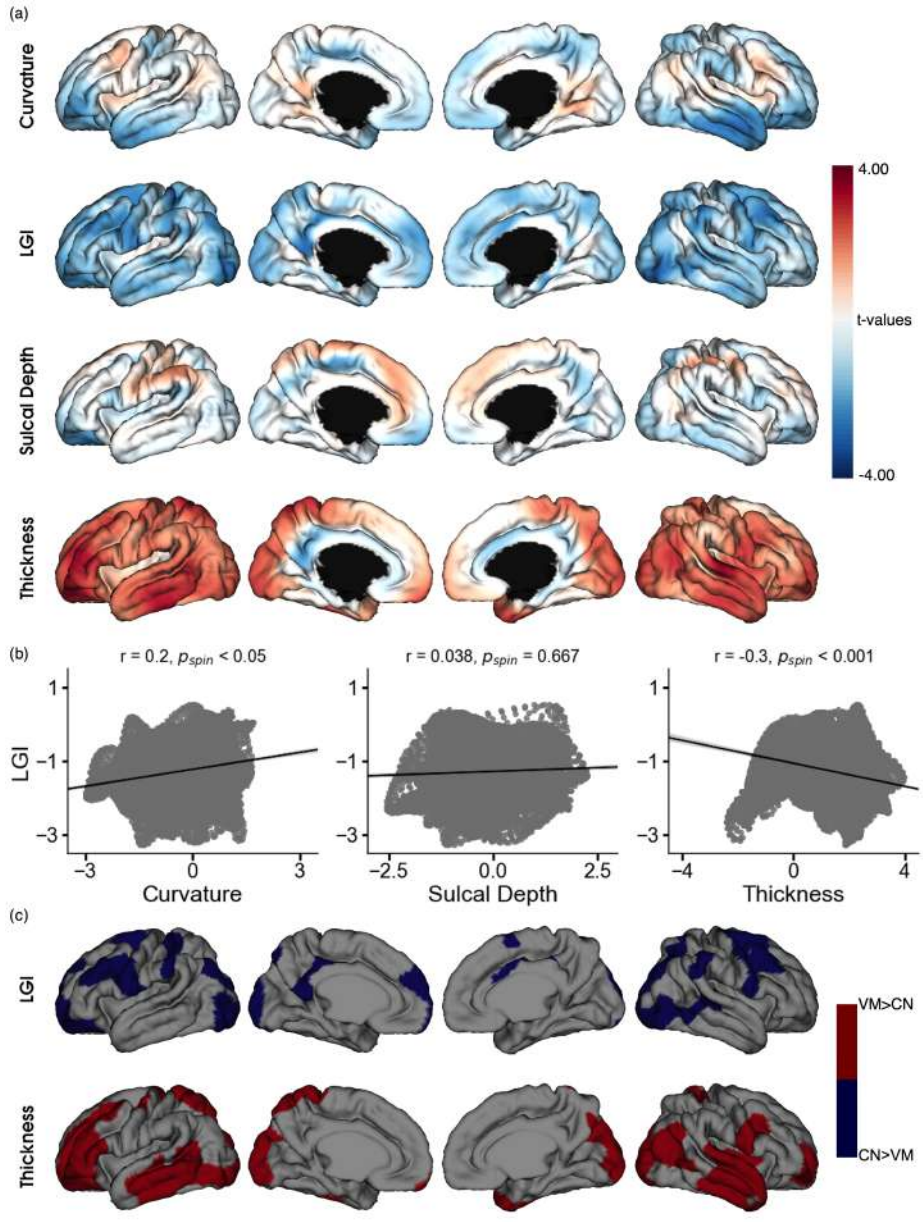
(a)
Curvature
LGI
Sulcal Depth
Thickness
4.00
t-values
-4.00
(b)
r = 0.2, p_{spin} < 0.05
r = 0.038, p_{spin} = 0.667
r = -0.3, p_{spin} < 0.001
LGI
Curvature
Sulcal Depth
Thickness
(c)
LGI
Thickness
VM>CN
CN>VM

Figure 3.4: Vertex-wise morphometric analysis. (a) T-maps of group-wise differences in mean curvature, local gyrification index, sulcal depth and cortical thickness respectively, computed using vertex-wise mixed-effects models. (b) Correlations of the t-map of local gyrification index with those of mean curvature, sulcal depth and cortical thickness. Significance is assessed using spin tests based on 1000 permutations. (c) Significant clusters (thresholded for a minimum size over 50 vertices) for LGI and cortical thickness. Red clusters denote regions with higher values in VM subjects than in controls, whereas blue clusters represent regions with lower values in VM subjects than in controls.

3.4 Discussion

In this work, we presented a longitudinal neuroimaging analysis of the relationship between ventricular enlargement and cortical development from fetal to the neonatal period. Our study is based on a dataset composed of 30 subjects (15 healthy controls and 15 subjects diagnosed with INSVM), each of which underwent both fetal and neonatal MRI. Subjects with VM showed consistently higher lateral ventricular volumes compared with healthy controls at both timepoints, with ventricular volumes generally increasing when going from fetal to the neonatal stage. To provide an accurate depiction of the relationship between VM and cortical development, the latter was characterized using volumetric measurements as well as cortical thickness and several descriptors of gyrification (i.e., mean curvature, sulcal depth and local gyrification index). Based on these features, the impact of ventricular dilation on cortical development was assessed both globally and locally in order to potentially identify more localized regions in the cortex with alterations in cortical development. Cortex-wise, our results show slightly higher cortical volumes and generally reduced cortical folding in subjects with VM compared to healthy controls, although significant differences were only found in neonates when using mean curvature and local gyrification index. At a more fine-grained level, our analyses coincided in highlighting a cortical overgrowth and a reduced

development in cortical regions of the cingulate gyrus, and in the frontal, occipital and parietal lobes. This delayed cortical development in subjects with VM was manifested in decreased gyrification, and an increase in cortical volume and thickness.

The impact of VM on cortical development and brain functionality has been extensively investigated in the literature. Previous studies showed that the risk of neurological abnormality in INSVM is above 10% Gaglioti et al. (2009); Garel (2004); Mehta and Levine (2005). INSVM has been observed to be related to higher risks of autism, attention-deficit and hyperactivity disorders Ball et al. (2013); Gilmore et al. (2001), and cognitive, language, and behavior deficits Leitner et al. (2009); Lyall et al. (2012); Sadan et al. (2007), generally related to a delayed neurodevelopment. To establish and quantify the impact of fetal VM in cortical development from the gestational to the post-natal period, we analysed ventricular growth in healthy and VM subjects using our longitudinal cohort. Here, we observed a general growth in volume of lateral ventricles through time, which is in line with the findings present in the literature Cutler et al. (2020); Ma et al. (2019). Differences were observed between the groups, in particular larger lateral ventricular volumes were found in subjects with VM with respect to healthy controls at both timepoints (i.e., fetal and neonatal stage). Not only ventricular volume was consistently larger, but we could also observe a difference in growth rate, with ventricular volume in VM subjects increasing more compared to healthy subjects in the same temporal window.

Some works have shown a relationship between VM and cortical overgrowth alongside specific pathologies such as Sotoâs syndrome Leventopoulos et al. (2009); Palmen et al. (2005), hemimegalencephaly Kalifa et al. (1987), and autism Palmen et al. (2005). The emergence of these apparent connections has led to the study of the relationship between VM and cortical folding alterations. Kyriakopoulou et al. (2014) reported an effective cortical overgrowth in fetuses with VM with respect to healthy controls. In neonates, Gilmore et al. (2008) also showed that subjects with INSVM had significantly larger cortical volumes than control subjects,

with no significant differences in absolute white matter volume. Lyall et al. (2012) found that ventricular enlargement persisted at the age of 2 years and was then associated with increases in both gray and white matter volumes. In these works, the authors suggested that ventricular enlargement, and subsequently an increase in surface area, may result in a larger number of progenitor neurons, influencing cortical volume. A larger number of cortical neurons with respect to control subjects has been observed in subjects with autism Courchesne et al. (2011b), which in several works have been demonstrated to present cortical overgrowth Courchesne et al. (2011a); Hazlett et al. (2011); Palmen et al. (2005) through their life-span. In our study, we found significant longitudinal differences in volume in the cingulate gyri and in the frontal, occipital and parietal lobes. These findings are in alignment with the literature Kyriakopoulou et al. (2014), highlighting an overgrowth in the cortex and in other tissues (i.e., white matter, thalami). Higher cortical volumes might suggest a delayed cortical development in VM subjects with respect to healthy subjects.

To assess whether there is an effective reduction in cortical development, we also analysed group-wise differences in several cortical folding descriptors (i.e., local gyrification index, mean curvature and sulcal depth) and thickness. Recently, some studies have shown associations between reduced curvature and ventricular dilation in fetuses Benkarim et al. (2018b); Scott et al. (2013) in brain regions such as the parietal and occipital lobes. In particular, Scott et al. (2013) found significant differences in mean curvature in the parieto-occipital sulcus in subjects affected by mild VM, whereas Benkarim et al. (2018b) reported reduced values of different measures of curvature in insula, parietal and occipital lobes in subjects diagnosed with INSVM. Our results are in accordance with the findings present in literature, showing an increased cortical thickness and reduced folding in VM subjects with respect to healthy controls in the frontal, occipital and parietal lobes. In particular, observing these regions in time, we found that LGI had a significantly positive correlation with curvature and a negative correlation with thickness. These results suggest the presence of a delay in growth in the last stage of pregnancy, where most of the

gyrification and cortical development take place Clouchoux et al. (2012).

A limitation of the present study is the small size of the dataset. Ideally, more subjects would be needed to investigate the differences at each timepoint and especially at late-onset stage. Nonetheless, the peculiarity of the collected dataset is represented by the multiple MRI acquisitions at fetal and neonatal stage, which makes it difficult to have larger numbers. Moreover, perinatal segmentation is subject to challenges related to myelination and the rapid changes in shape and size occurring during this stage of brain development, which make it difficult to accurately segment the different brain tissues and structures using existing methods. As a future work, the study could be extended to investigate different volumetric and cortical folding descriptors in larger datasets. Moreover, our results could also be used to study the relationship between cortical folding and neurobehavioural test scores that assess cognitive and functional skills in neonates.

To conclude, our work investigated the relationship between VM and cortical development in a longitudinal cohort including both fetuses and neonates. Our analyses showed longitudinally significant decreases in cortical development in subjects with VM compared to healthy controls. This delay in cortical development was consistently found across multiple descriptors, translating into reduced cortical folding, cortical volume overgrowth, and thicker cortices in VM subjects. Our findings further indicated that the delay in cortical development was bilaterally confined to the cingulate cortex as well as to regions within the frontal, occipital and parietal lobes. To the best of our knowledge, this is the first longitudinal MRI study to investigate the impact of VM on cortical development in the temporal window spanning the intrauterine and postnatal period. Our work further confirms and consolidates the findings of previous cross-sectional studies indicating a reduced cortical folding in fetuses with VM.

Chapter 4

CONCLUSIONS

After an introduction on perinatal brain development and existing perinatal analysis tools, this thesis has presented novel approaches to study fetal and neonatal brain. First, we proposed a newly developed automatic segmentation and surface extraction pipeline for fetal and neonatal brains, and we evaluated it on fetal and neonatal data against state of the art methods. Second, we used the pipeline to compute brain tissue and structural segmentation and extract volumetric features and cortical folding descriptors, and analyzed brain development and the deviations from its normative course in the presence of ventriculomegaly, which is the most common abnormal finding in the fetal brain, from fetal to neonatal stage.

4.1 Research summary

4.1.1 Segmentation and cortical surface extraction

Challenges in perinatal brain segmentation, introduced by limitations such as intensity inhomogeneities, noise and partial volume effects, made the subject particularly interesting in research over the years. In the state of the art, these challenges are tackled using different strategies. In most of the cases, fetal or neonatal brains are segmented adopting temporal atlases, in particular registering the subject to the corresponding target at the same gestational age. This makes the final result strictly dependent on age, whereas one of the most critical aspects of this particular developmental phase is the fast, highly variable growth that the brain undergoes. In case of multi-subject atlases, the final result is computed through label fusion, and thus based on the similarity metric between the subject and each sample after registration: this method is more robust in terms of age dependency, but it is limited by the characteristics of the atlas (i.e.: number of subjects composing it, their age range and variance, the similarity of the subject to the data composing the atlas itself). Moreover, the size of the atlas directly affects the computational load as the subject needs to be registered to each of the samples composing the atlas. In this thesis, we propose a methodological approach combining the two solutions and introducing a registration approach that makes the process scalable without increasing

dramatically the computational load.

In Chapter 2, the thesis presents a new pipeline for the structural segmentation and cortical surface extraction of fetal and neonatal brain MRI. We introduced a fetal temporal template, used to compute tissue priors for the subject by non-rigid registration to the age-corresponding sample in the template. In the second step of the computation, a new multi-subject fetal atlas is used to compute the final tissue and structural segmentation, using a three-channel registration between the subject and an average template. Here, combining the resulting transformation to a previously computed transformation between each sample composing the atlas and the average template, we obtained the transformation between the subject and each sample of the atlas minimising the number of registrations. The final label fusion-based segmentations are computed assigning a weight to each transformation, based on a similarity metric. Finally, the cortical surface is extracted and cortical folding features and thickness are computed from the regularised mesh. The pipeline allows for a consistent and coherent fetal and neonatal segmentation in the same framework. Results show how the segmentation accuracy was enhanced by using fetal templates for all the main tissues: considering both the cortical shape and the ventricles in the registration leads to more accurate outcomes with respect to only taking into account the cortical shape. Moreover, for both neonatal and fetal acquisitions, performances were dramatically improved, and the approaches presented make the process scalable as the size of the atlas could be increased without affecting the computational load. The possibility of computing a structural and regional segmentation for both fetal and neonatal images, and to extract the cortical surface and its folding descriptors, opens a variety of possible clinical applications for the pipeline.

4.1.2 Analysis of neurodevelopment in ventriculomegaly

The study of the effect of ventriculomegaly on neurodevelopment at different developmental stages has drawn significant attention in clinical research. Connections between an abnormal ventricular enlargement and cortical overgrowth have been observed both in fetuses and neonates, as

well as reduced folding, identified through cortical descriptors such as curvature and thickness. Despite being a topic thoroughly explored, it remains unclear what is the relationship between ventriculomegaly and cortical abnormal development through time.

In Chapter 3, we carried out a study to assess the relationship between ventriculomegaly and cortical development using a longitudinal dataset composed of 30 subjects, of which 15 with ventriculomegaly and 15 healthy controls. For each of these subjects, one brain MRI scan was acquired during gestation and one post-natal, for a total of 60 scans. We were able to compute both a tissue and a structural segmentation for all the acquired data using the previously presented pipeline, as well as the cortical mesh and its cortical folding descriptors. By means of a surface coregistration algorithm, surfaces were topologically aligned and normalised to the same size. The analysis we carried out consisted of three phases. First, we studied global differences between groups by investigating global volumetric features, in particular total ventricular and cortical volumes, and globally averaged cortical descriptors at each stage (i.e.: at fetal and neonatal stage). In the second phase, we analysed differences in lobular volumes at each stage separately and longitudinally by means of mixed-effect models, in which we predicted each lobe volume taking into account multiple acquisitions for a single subject and using age and sex as covariates. Finally, in the third phase, we conducted a vertex-wise analysis of the cortical features. In particular, using mixed-effect models, we investigated differences in cortical folding descriptors, such as mean curvature, local gyrification index, sulcal depth and thickness.

From the findings of our study, we can conclude that ventriculomegaly is better characterized by ventricular volume, which captures the extent of dilation, than diagnosis. Moreover, these findings also suggest stronger ipsilateral than global relationships, as our hemispheric analyses showed to capture more significant associations. The second approach further confirmed the findings of our statistical analyses, highlighting relevant associations found between ventriculomegaly and altered cortical folding in the insula, the parietal lobe and the posterior part of the temporal lobe.

From the findings of our study, we can conclude that an abnormal

cortical development can be observed longitudinally in subjects with VM compared to healthy controls. In particular, we observe a decrease in cortical folding and a cortical volume overgrowth over time, with thicker, less convoluted cortices. More specifically, areas affected by the abnormal development were identified within the cingulate cortex and in the frontal, occipital and parietal lobes. This work further confirms and consolidates the findings of previous cross-sectional studies indicating a reduced cortical folding during early development in subjects with VM.

4.2 Future research directions

Differences in shape, size as well as intensity distribution of the MRI scan can translate into registration errors, especially in the investigated temporal window, when acquisition and processing of the MR images presents several challenges related to the fast development of the brain. In the presented pipeline, two multi-subject atlases have been used, each one composed of 20 subjects, for fetal and neonatal structural and tissue segmentation. In the investigated temporal window, though, differences can be dramatic between two subjects relatively close in age, thus increasing the size and the variability of the atlas could improve the results. In particular, the proposed approach for registration makes the process scalable, meaning that the size of the atlas could be increased without affecting the computational load. This represents a possible line of future work, alongside newly developed, faster approaches for registration, such as deep learning-based techniques. Indeed, traditional registration remains a computationally expensive process, a limitation that has been overcome in the present work by minimising the amount of pairwise registrations performed for the segmentation.

In the analysis of the impact of ventriculomegaly on brain development, our work investigated associations of ventricular dilation with cortical folding and volumetric development both globally and locally. Compared to previous works covering this specific developmental stage, a vertex-wise analysis of a wide set of cortical folding descriptors has been carried out,

confirming the previous findings and additionally studying the longitudinal effect of ventriculomegaly on cortical development. The reduced size of the dataset, though, remains a limitation. As a future line of work, a wider dataset should be investigated, with different cortical folding measures, to find other possible associations. Moreover, as a follow-up to this study, to assess the prognostic power of the analysed features, it would be interesting to investigate the existing relationship between cortical folding and neurobehavioural markers used to assess cognitive and functional skills in neonates.

Bibliography

Alexander, B., Murray, A. L., Loh, W. Y., Matthews, L. G., Adamson, C., Beare, R., Chen, J., Kelly, C. E., Rees, S., Warfield, S. K., et al. (2017). A new neonatal cortical and subcortical brain atlas: the Melbourne Children's Regional Infant Brain (M-CRIB) atlas. *NeuroImage*, 147:841–851.

Alexander-Bloch, A. F., Shou, H., Liu, S., Satterthwaite, T. D., Glahn, D. C., Shinohara, R. T., Vandekar, S. N., and Raznahan, A. (2018). On testing for spatial correspondence between maps of human brain structure and function. *Neuroimage*, 178:540–551.

Amlien, I. K., Fjell, A. M., Tamnes, C. K., Grydeland, H., Krogsrud, S. K., Chaplin, T. A., Rosa, M. G., and Walhovd, K. B. (2016). Organizing principles of human cortical developmentâthickness and area from 4 to 30 years: insights from comparative primate neuroanatomy. *Cerebral cortex*, 26(1):257–267.

Armstrong, E., Schleicher, A., Omran, H., Curtis, M., and Zilles, K. (1995). The ontogeny of human gyrification. *Cerebral cortex*, 5(1):56–63.

Avants, B. B., Tustison, N., Song, G., et al. (2009). Advanced normalization tools (ANTS). *Insight j*, 2(365):1–35.

Ball, J. D., Abuhamad, A. Z., Mason, J. L., Burket, J., Katz, E., and Deutsch, S. I. (2013). Clinical outcomes of mild isolated cerebral ventriculomegaly in the presence of other neurodevelopmental risk factors. *Journal of Ultrasound in Medicine*, 32(11):1933–1938.

Belaroussi, B., Milles, J., Carme, S., Zhu, Y. M., and Benoit-Cattin, H. (2006). Intensity non-uniformity correction in MRI: existing methods and their validation. *Medical image analysis*, 10(2):234–246.

Benkarim, O., Piella, G., Rekik, I., Hahner, N., Eixarch, E., Shen, D., Li, G., González Ballester, M. A., and Sanroma, G. (2020). A novel approach to multiple anatomical shape analysis: Application to fetal ventriculomegaly. *Medical Image Analysis*, 64:101750.

Benkarim, O. M., Hahner, N., Piella, G., Gratacos, E., González Ballester, M. A., Eixarch, E., and Sanroma, G. (2018a). Cortical folding alterations in fetuses with isolated non-severe ventriculomegaly. *NeuroImage: Clinical*, 18:103–114.

Benkarim, O. M., Sanroma, G., Piella, G., Rekik, I., Hahner, N., Eixarch, E., González Ballester, M. A., Shen, D., and Li, G. (2018b). Revealing Regional Associations of Cortical Folding Alterations with In Utero Ventricular Dilation Using Joint Spectral Embedding. In *Medical Image Computing and Computer Assisted Intervention – MICCAI 2018*, pages 620–627, Cham. Springer International Publishing.

Benkarim, O. M., Sanroma, G., Zimmer, V. A., Muñoz Moreno, E., Hahner, N., Eixarch, E., Camara, O., González Ballester, M. A., and Piella, G. (2017). Toward the automatic quantification of in utero brain development in 3D structural MRI: A review. *Human Brain Mapping*, 38(5):2772–2787.

Besl, P. and McKay, N. D. (1992). A method for registration of 3-D shapes. *IEEE Transactions on Pattern Analysis and Machine Intelligence*, 14(2):239–256.

Boardman, J. P., Craven, C., Valappil, S., Counsell, S. J., Dyet, L. E., Rueckert, D., Aljabar, P., Rutherford, M. A., Chew, A. T., Allsop, J. M., et al. (2010). A common neonatal image phenotype predicts adverse neurodevelopmental outcome in children born preterm. *Neuroimage*, 52(2):409–414.

Brown, T. T., Kuperman, J. M., Chung, Y., Erhart, M., McCabe, C., Hagler Jr, D. J., Venkatraman, V. K., Akshoomoff, N., Amaral, D. G., Bloss, C. S., et al. (2012). Neuroanatomical assessment of biological maturity. *Current biology*, 22(18):1693–1698.

Cawley, P., Few, K., Greenwood, R., Malcolm, P., Johnson, G., Lally, P., Thayyil, S., and Clarke, P. (2016). Does magnetic resonance brain scanning at 3.0 tesla pose a hyperthermic challenge to term neonates? *The Journal of pediatrics*, 175:228–230.

Chi, J. G., Dooling, E. C., and Gilles, F. H. (1977). Gyral development of the human brain. *Annals of Neurology: Official Journal of the American Neurological Association and the Child Neurology Society*, 1(1):86–93.

Clark, W. E. L. G. (1945). *Deformation patterns in the cerebral cortex*. Printed at the Oxford University Press by John Johnson.

Clouchoux, C., Du Plessis, A., Bouyssi-Kobar, M., Tworetzky, W., McElhinney, D., Brown, D., Gholipour, A., Kudelski, D., Warfield, S., McCarter, R., et al. (2013). Delayed cortical development in fetuses with complex congenital heart disease. *Cerebral cortex*, 23(12):2932–2943.

Clouchoux, C., Kudelski, D., Gholipour, A., Warfield, S. K., Viseur, S., Bouyssi-Kobar, M., Mari, J.-L., Evans, A. C., Du Plessis, A. J., and Limperopoulos, C. (2012). Quantitative in vivo MRI measurement of cortical development in the fetus. *Brain Structure and Function*, 217(1):127–139.

Counsell, S. J., Edwards, A. D., Chew, A. T., Anjari, M., Dyet, L. E., Srinivasan, L., Boardman, J. P., Allsop, J. M., Hajnal, J. V., Rutherford, M. A., et al. (2008). Specific relations between neurodevelopmental abilities and white matter microstructure in children born preterm. *Brain*, 131(12):3201–3208.

Courchesne, E., Campbell, K., and Solso, S. (2011a). Brain growth across the life span in autism: age-specific changes in anatomical pathology. *Brain research*, 1380:138–145.

Courchesne, E., Mouton, P. R., Calhoun, M. E., Semendeferi, K., Ahrens-Barbeau, C., Hallet, M. J., Barnes, C. C., and Pierce, K. (2011b). Neuron number and size in prefrontal cortex of children with autism. *Jama*, 306(18):2001–2010.

Crovetto, F., Crispi, F., Casas, R., Martín-Asuero, A., Borràs, R., Vieta, E., Estruch, R., Gratacós, E., Paules, C., Nakaki, A., et al. (2021). Effects of Mediterranean Diet or Mindfulness-Based Stress Reduction on Prevention of Small-for-Gestational Age Birth Weights in Newborns Born to At-Risk Pregnant Individuals: The IMPACT BCN Randomized Clinical Trial. *JAMA*, 326(21):2150–2160.

Cutler, N. S., Srinivasan, S., Aaron, B. L., Anand, S. K., Kang, M. S., Altshuler, D. B., Schermerhorn, T. C., Hollon, T. C., Maher, C. O., and Khalsa, S. S. S. (2020). Normal cerebral ventricular volume growth in childhood. *Journal of Neurosurgery: Pediatrics*, 26(5):517–524.

D'Addario, V. (2017). Fetal diagnosis and therapy: a continously evolving discipline. *Journal of Perinatal Medicine*, 45(2):147–148.

de Dumast, P., Kebiri, H., Atat, C., Dunet, V., Koob, M., and Cuadra, M. B. (2020). Segmentation of the cortical plate in fetal brain MRI with a topological loss.

Dubois, J., Alison, M., Counsell, S. J., Hertz-Pannier, L., Hüppi, P. S., and Benders, M. J. (2021). MRI of the neonatal brain: a review of methodological challenges and neuroscientific advances. *Journal of Magnetic Resonance Imaging*, 53(5):1318–1343.

Ebner, M., Chung, K. K., Prados, F., Cardoso, M. J., Chard, D. T., Vercauteren, T., and Ourselin, S. (2018a). Volumetric reconstruction from printed films: Enabling 30 year longitudinal analysis in MR neuroimaging. *NeuroImage*, 165:238–250.

Ebner, M., Wang, G., Li, W., Aertsen, M., Patel, P., Aughwane, R., Melbourne, A., Doel, T., Dymarkowski, S., David, A., Deprest, J., Ourselin,

S., and Vercauteren, T. (2019). An automated framework for localization, segmentation and super-resolution reconstruction of fetal brain MRI. *NeuroImage*, 206:116324.

Ebner, M., Wang, G., Li, W., Aertsen, M., Patel, P. A., Aughwane, R., Melbourne, A., Doel, T., David, A. L., Deprest, J., Ourselin, S., and Vercauteren, T. (2018b). An Automated Localization, Segmentation and Reconstruction Framework for Fetal Brain MRI. In *Medical Image Computing and Computer Assisted Intervention – MICCAI 2018*, pages 313–320, Cham. Springer International Publishing.

Essen, D. C. v. (1997). A tension-based theory of morphogenesis and compact wiring in the central nervous system. *Nature*, 385(6614):313–318.

Fernández, V., Llinares-Benadero, C., and Borrell, V. (2016). Cerebral cortex expansion and folding: what have we learned? *The EMBO journal*, 35(10):1021–1044.

Fischl, B., Rajendran, N., Busa, E., Augustinack, J., Hinds, O., Yeo, B. T., Mohlberg, H., Amunts, K., and Zilles, K. (2008). Cortical folding patterns and predicting cytoarchitecture. *Cerebral cortex*, 18(8):1973–1980.

Gaglioti, P., Oberto, M., and Todros, T. (2009). The significance of fetal ventriculomegaly: etiology, short-and long-term outcomes. *Prenatal Diagnosis: Published in Affiliation with the International Society for Prenatal Diagnosis*, 29(4):381–388.

Garel, C. (2004). Ventricular dilatation. In *MRI of the Fetal Brain*, pages 201–216. Springer.

Garel, C. (2008). Imaging the fetus: when does MRI really help? *Pediatric radiology*, 38:467.

Gholipour, A., Rollins, C. K., Velasco-Annis, C., Ouaalam, A., Akhondi-Asl, A., Afacan, O., Ortinau, C. M., Clancy, S., Limperopoulos, C.,

Yang, E., Estroff, J. A., and Warfield, S. K. (2017). A normative spatiotemporal MRI atlas of the fetal brain for automatic segmentation and analysis of early brain growth. *Sci Rep*, 7(1):476.

Gilmore, J. H., Smith, L. C., Wolfe, H. M., Hertzberg, B. S., Smith, J. K., Chescheir, N. C., Evans, D. D., Kang, C., Hamer, R. M., Lin, W., et al. (2008). Prenatal mild ventriculomegaly predicts abnormal development of the neonatal brain. *Biological psychiatry*, 64(12):1069–1076.

Gilmore, J. H., van Tol, J. J., Streicher, H. L., Williamson, K., Cohen, S. B., Greenwood, R. S., Charles, H. C., Kliewer, M. A., Whitt, J. K., Silva, S. G., et al. (2001). Outcome in children with fetal mild ventriculomegaly: a case series. *Schizophrenia research*, 48(2-3):219–226.

Glastonbury, C. M. and Kennedy, A. M. (2002). Ultrafast MRI of the fetus. *Australasian radiology*, 46(1):22–32.

Glenn, O. A. (2010). MR imaging of the fetal brain. *Pediatric radiology*, 40(1):68–81.

Gómez-Arriaga, P., Herraiz, I., Puente, J. M., Zamora-Crespo, B., Núñez-Enamorado, N., and Galindo, A. (2012). Mid-term neurodevelopmental outcome in isolated mild ventriculomegaly diagnosed in fetal life. *Fetal diagnosis and therapy*, 31(1):12–18.

González Ballester, M. A., Zisserman, A., and Brady, M. (2000). Segmentation and measurement of brain structures in MRI including confidence bounds. *Medical Image Analysis*, 4(3):189–200.

González Ballester, M. A., Zisserman, A. P., and Brady, M. (2002). Estimation of the partial volume effect in MRI. *Medical image analysis*, 6(4):389–405.

Gousias, I. S., Edwards, A. D., Rutherford, M. A., Counsell, S. J., Hajnal, J. V., Rueckert, D., and Hammers, A. (2012). Magnetic resonance imaging of the newborn brain: manual segmentation of labelled atlases in term-born and preterm infants. *Neuroimage*, 62(3):1499–1509.

Gousias, I. S., Hammers, A., Counsell, S. J., Srinivasan, L., Rutherford, M. A., Heckemann, R. A., Hajnal, J. V., Rueckert, D., and Edwards, A. D. (2013a). Magnetic resonance imaging of the newborn brain: automatic segmentation of brain images into 50 anatomical regions. *PloS one*, 8(4):e59990.

Gousias, I. S., Hammers, A., Counsell, S. J., Srinivasan, L., Rutherford, M. A., Heckemann, R. A., Hajnal, J. V., Rueckert, D., and Edwards, A. D. (2013b). Magnetic Resonance Imaging of the Newborn Brain: Automatic Segmentation of Brain Images into 50 Anatomical Regions. *PLOS ONE*, 8(4):1–16.

Griffiths, P., Reeves, M., Morris, J., Mason, G., Russell, S., Paley, M., and Whitby, E. (2010). A prospective study of fetuses with isolated ventriculomegaly investigated by antenatal sonography and in utero MR imaging. *American journal of neuroradiology*, 31(1):106–111.

Griffiths, P. D., Bradburn, M., Campbell, M. J., Cooper, C. L., Embleton, N., Graham, R., Hart, A. R., Jarvis, D., Kilby, M. D., Lie, M., et al. (2019). MRI in the diagnosis of fetal developmental brain abnormalities: the MERIDIAN diagnostic accuracy study. *Health Technology Assessment*.

Habas, P. A., Kim, K., Corbett-Detig, J. M., Rousseau, F., Glenn, O. A., Barkovich, A. J., and Studholme, C. (2010). A spatiotemporal atlas of MR intensity, tissue probability and shape of the fetal brain with application to segmentation. *Neuroimage*, 53(2):460–470.

Hahner, N., Benkarim, O., Aertsen, M., Perez-Cruz, M., Piella, G., Sanroma, G., Bargallo, N., Deprest, J., Ballester, M. G., Gratacos, E., et al. (2019). Global and regional changes in cortical development assessed by MRI in fetuses with isolated nonsevere ventriculomegaly correlate with neonatal neurobehavior. *American Journal of Neuroradiology*, 40(9):1567–1574.

Hazlett, H. C., Poe, M. D., Gerig, G., Styner, M., Chappell, C., Smith, R. G., Vachet, C., and Piven, J. (2011). Early brain overgrowth in autism

associated with an increase in cortical surface area before age 2 years. *Archives of general psychiatry*, 68(5):467–476.

Hilgetag, C. C. and Barbas, H. (2006). Role of mechanical factors in the morphology of the primate cerebral cortex. *PLoS computational biology*, 2(3):e22.

Huisman, T. A., Tekes, A., and Poretti, A. (2012). Brain malformations and fetal ventriculomegaly: what to look for? *Journal of Pediatric Neuroradiology*, 1(3):185–195.

Jackson, D. C., Irwin, W., Dabbs, K., Lin, J. J., Jones, J. E., Hsu, D. A., Stafstrom, C. E., Seidenberg, M., and Hermann, B. P. (2011). Ventricular enlargement in new-onset pediatric epilepsies. *Epilepsia*, 52(12):2225–2232.

Jou, R. J., Hardan, A. Y., and Keshavan, M. S. (2005). Reduced cortical folding in individuals at high risk for schizophrenia: a pilot study. *Schizophrenia research*, 75(2-3):309–313.

Kainz, B., Keraudren, K., Kyriakopoulou, V., Rutherford, M., Hajnal, J. V., and Rueckert, D. (2014). Fast fully automatic brain detection in fetal MRI using dense rotation invariant image descriptors. In *2014 IEEE 11th International Symposium on Biomedical Imaging (ISBI)*, pages 1230–1233. IEEE.

Kalifa, G., Chiron, C., Sellier, N., Demange, P., Ponsot, G., Lalande, G., and Robain, O. (1987). Hemimegalencephaly: MR imaging in five children. *Radiology*, 165(1):29–33.

Keraudren, K., Kuklisova-Murgasova, M., Kyriakopoulou, V., Malamateniou, C., Rutherford, M. A., Kainz, B., Hajnal, J. V., and Rueckert, D. (2014). Automated fetal brain segmentation from 2D MRI slices for motion correction. *NeuroImage*, 101:633–643.

Kim, K., Habas, P. A., Rousseau, F., Glenn, O. A., Barkovich, A. J., and Studholme, C. (2009). Intersection based motion correction of multislice

MRI for 3-D in utero fetal brain image formation. *IEEE transactions on medical imaging*, 29(1):146–158.

King, J. B., Lopez-Larson, M. P., and Yurgelun-Todd, D. A. (2016). Mean cortical curvature reflects cytoarchitecture restructuring in mild traumatic brain injury. *NeuroImage: Clinical*, 11:81–89.

Kneeland, J., Shimakawa, A., and Wehrli, F. (1986). Effect of intersection spacing on MR image contrast and study time. *Radiology*, 158(3):819–822.

Kriegstein, A., Noctor, S., and Martínez-Cerdeño, V. (2006). Patterns of neural stem and progenitor cell division may underlie evolutionary cortical expansion. *Nature Reviews Neuroscience*, 7(11):883–890.

Kuklisova-Murgasova, M., Aljabar, P., Srinivasan, L., Counsell, S. J., Doria, V., Serag, A., Gousias, I. S., Boardman, J. P., Rutherford, M. A., Edwards, A. D., et al. (2011). A dynamic 4D probabilistic atlas of the developing brain. *NeuroImage*, 54(4):2750–2763.

Kuklisova-Murgasova, M., Quaghebeur, G., Rutherford, M. A., Hajnal, J. V., and Schnabel, J. A. (2012). Reconstruction of fetal brain MRI with intensity matching and complete outlier removal. *Medical image analysis*, 16(8):1550–1564.

Kyriakopoulou, V., Vatansever, D., Elkommos, S., Dawson, S., McGuinness, A., Allsop, J., Molnár, Z., Hajnal, J., and Rutherford, M. (2014). Cortical overgrowth in fetuses with isolated ventriculomegaly. *Cerebral Cortex*, 24(8):2141–2150.

Landrieu, P., Husson, B., Pariente, D., and Lacroix, C. (1998). MRI-neuropathological correlations in type 1 lissencephaly. *Neuroradiology*, 40(3):173–176.

Lefèvre, J. and Mangin, J.-F. (2010). A reaction-diffusion model of human brain development. *PLoS computational biology*, 6(4):e1000749.

Leitner, Y., Stolar, O., Rotstein, M., Toledano, H., Harel, S., Bitchonsky, O., Ben-Adani, L., Miller, E., and Ben-Sira, L. (2009). The neurocognitive outcome of mild isolated fetal ventriculomegaly verified by prenatal magnetic resonance imaging. *American journal of obstetrics and gynecology*, 201(2):215–e1.

Leventopoulos, G., Kitsiou-Tzeli, S., Kritikos, K., Psoni, S., Mavrou, A., Kanavakis, E., and Fryssira, H. (2009). A clinical study of Sotos syndrome patients with review of the literature. *Pediatric neurology*, 40(5):357–364.

Lyall, A. E., Woolson, S., Wolfe, H. M., Goldman, B. D., Reznick, J. S., Hamer, R. M., Lin, W., Styner, M., Gerig, G., and Gilmore, J. H. (2012). Prenatal isolated mild ventriculomegaly is associated with persistent ventricle enlargement at ages 1 and 2. *Early human development*, 88(8):691–698.

Lyu, I., Kim, S. H., Girault, J. B., Gilmore, J. H., and Styner, M. A. (2018). A cortical shape-adaptive approach to local gyrification index. *Medical image analysis*, 48:244–258.

Ma, H.-L., Zhao, S.-X., Lv, F.-R., Zhang, Z.-W., Xiao, Y.-H., and Sheng, B. (2019). Volume growth trend and correlation of atrial diameter with lateral ventricular volume in normal fetus and fetus with ventriculomegaly: A STROBE compliant article. *Medicine*, 98(26).

Makropoulos, A., Aljabar, P., Wright, R., Hüning, B., Merchant, N., Arichi, T., Tusor, N., Hajnal, J. V., Edwards, A. D., Counsell, S. J., et al. (2016). Regional growth and atlasing of the developing human brain. *Neuroimage*, 125:456–478.

Makropoulos, A., Counsell, S., and Rueckert, D. (2017). A review on automatic fetal and neonatal brain MRI segmentation. *NeuroImage*.

Makropoulos, A., Ledig, C., Aljabar, P., Serag, A., Hajnal, J. V., Edwards, A. D., Counsell, S. J., and Rueckert, D. (2012). Automatic tissue

and structural segmentation of neonatal brain MRI using expectation-maximization. *MICCAI Grand Challenge on Neonatal Brain Segmentation*, 2012:9–15.

Makropoulos, A., Robinson, E., Schuh, A., Wright, R., Fitzgibbon, S., Bozek, J., Counsell, S., Steinweg, J., Vecchiato, K., Passerat-Palmbach, J., Lenz, G., Mortari, F., Tenev, T., Duff, E., Bastiani, M., Cordero-Grande, L., Hughes, E., Tusor, N., Tournier, J.-D., and Rueckert, D. (2018). The developing human connectome project: A minimal processing pipeline for neonatal cortical surface reconstruction. *NeuroImage*, 173.

Malamateniou, C., Malik, S., Counsell, S., Allsop, J., McGuinness, A., Hayat, T., Broadhouse, K., Nunes, R., Ederies, A., Hajnal, J., et al. (2013). Motion-compensation techniques in neonatal and fetal MR imaging. *American Journal of Neuroradiology*, 34(6):1124–1136.

Mehta, T. S. and Levine, D. (2005). Imaging of fetal cerebral ventriculomegaly: a guide to management and outcome. In *Seminars in Fetal and Neonatal Medicine*, volume 10, pages 421–428. Elsevier.

Melchiorre, K., Bhide, A., Gika, A., Pilu, G., and Papageorghiou, A. (2009). Counseling in isolated mild fetal ventriculomegaly. *Ultrasound in Obstetrics and Gynecology: The Official Journal of the International Society of Ultrasound in Obstetrics and Gynecology*, 34(2):212–224.

Milani, H. J. F., Barreto, E. Q. d. S., Araujo, E., Peixoto, A. B., Nardozza, L. M. M., and Moron, A. F. (2019). Ultrasonographic evaluation of the fetal central nervous system: review of guidelines. *Radiologia brasileira*, 52:176–181.

Moeskops, P., Viergever, M. A., Mendrik, A. M., De Vries, L. S., Benders, M. J., and Išgum, I. (2016). Automatic segmentation of MR brain images with a convolutional neural network. *IEEE transactions on medical imaging*, 35(5):1252–1261.

Nordahl, C. W., Dierker, D., Mostafavi, I., Schumann, C. M., Rivera, S. M., Amaral, D. G., and Van Essen, D. C. (2007). Cortical folding abnormalities in autism revealed by surface-based morphometry. *Journal of Neuroscience*, 27(43):11725–11735.

Oishi, K., Mori, S., Donohue, P. K., Ernst, T., Anderson, L., Buchthal, S., Faria, A., Jiang, H., Li, X., Miller, M. I., van Zijl, P. C., and Chang, L. (2011). Multi-contrast human neonatal brain atlas: Application to normal neonate development analysis. *NeuroImage*, 56(1):8–20.

Palmen, S. J., Pol, H. E. H., Kemner, C., Schnack, H. G., Durston, S., Lahuis, B. E., Kahn, R. S., and Van Engeland, H. (2005). Increased gray-matter volume in medication-naive high-functioning children with autism spectrum disorder. *Psychological medicine*, 35(4):561–570.

Payette, K., de Dumast, P., Kebiri, H., Ezhov, I., Paetzold, J. C., Shit, S., Iqbal, A., Khan, R., Kottke, R., Grehten, P., and et al. (2021). An automatic multi-tissue human fetal brain segmentation benchmark using the Fetal Tissue Annotation Dataset. *Scientific Data*, 8(1).

Payette, K., Kottke, R., and Jakab, A. (2020). Efficient multi-class fetal brain segmentation in high resolution MRI reconstructions with noisy labels.

Peterson, B. S., Anderson, A. W., Ehrenkranz, R., Staib, L. H., Tageldin, M., Colson, E., Gore, J. C., Duncan, C. C., Makuch, R., and Ment, L. R. (2003). Regional brain volumes and their later neurodevelopmental correlates in term and preterm infants. *Pediatrics*, 111(5):939–948.

Prastawa, M., Gilmore, J. H., Lin, W., and Gerig, G. (2005). Automatic segmentation of MR images of the developing newborn brain. *Medical image analysis*, 9(5):457–466.

Rajchl, M., Lee, M. C., Oktay, O., Kamnitsas, K., Passerat-Palmbach, J., Bai, W., Damodaram, M., Rutherford, M. A., Hajnal, J. V., Kainz, B., et al. (2016). Deepcut: Object segmentation from bounding box

annotations using convolutional neural networks. *IEEE transactions on medical imaging*, 36(2):674–683.

Rathbone, R., Counsell, S., Kapellou, O., Dyet, L., Kennea, N., Hajnal, J., Allsop, J., Cowan, F., and Edwards, A. (2011). Perinatal cortical growth and childhood neurocognitive abilities. *Neurology*, 77(16):1510–1517.

Raudenbush, S. W. and Bryk, A. S. (2002). *Hierarchical linear models: Applications and data analysis methods*, volume 1. sage.

Richman, D. P., Stewart, R. M., Hutchinson, J., and Caviness Jr, V. S. (1975). Mechanical Model of Brain Convolutional Development: Pathologic and experimental data suggest a model based on differential growth within the cerebral cortex. *Science*, 189(4196):18–21.

Rutherford, M. (2002). MRI of the Neonatal Brain. *Magnetic resonance imaging of the brain in preterm infants: 24 weeks' gestation to term*, pages 25–49.

Sadan, S., Malinger, G., Schweiger, A., Lev, D., and Lerman-Sagie, T. (2007). Neuropsychological outcome of children with asymmetric ventricles or unilateral mild ventriculomegaly identified in utero. *BJOG: An International Journal of Obstetrics & Gynaecology*, 114(5):596–602.

Saleem, S. N. (2014). Fetal MRI: An approach to practice: A review. *Journal of advanced research*, 5(5):507–523.

Salehi, S. S., Hashemi, S. R., Velasco-Annis, C., Ouaalam, A., Estroff, J., Erdogmus, D., Warfield, S., and Gholipour, A. (2018). Real-Time Automatic Fetal Brain Extraction in Fetal MRI by Deep Learning.

Sallet, P. C., Elkis, H., Alves, T. M., Oliveira, J. R., Sassi, E., de Castro, C. C., Busatto, G. F., and Gattaz, W. F. (2003). Reduced cortical folding in schizophrenia: an MRI morphometric study. *American Journal of Psychiatry*, 160(9):1606–1613.

Salomon, L., Bernard, J., and Ville, Y. (2007). Reference ranges for fetal ventricular width: a non-normal approach. *Ultrasound in obstetrics & gynecology*, 30(1):61–66.

Sanroma, G., Benkarim, O. M., Piella, G., and González Ballester, M. A. (2016). Building an ensemble of complementary segmentation methods by exploiting probabilistic estimates. In *International Workshop on Machine Learning in Medical Imaging*, pages 27–35. Springer.

Sanroma, G., Benkarim, O. M., Piella, G., Lekadir, K., Hahner, N., Eixarch, E., and González Ballester, M. A. (2018). Learning to combine complementary segmentation methods for fetal and 6-month infant brain MRI segmentation. *Computerized Medical Imaging and Graphics*, 69:52–59.

Schuh, A., Makropoulos, A., Wright, R., Robinson, E. C., Tusor, N., Steinweg, J., Hughes, E., Cordero Grande, L., Price, A., Hutter, J., Hajnal, J. V., and Rueckert, D. (2017). A deformable model for the reconstruction of the neonatal cortex. In *2017 IEEE 14th International Symposium on Biomedical Imaging (ISBI 2017)*, pages 800–803.

Schuh, A., Murgasova, M., Makropoulos, A., Ledig, C., Counsell, S. J., Hajnal, J. V., Aljabar, P., and Rueckert, D. (2014). Construction of a 4D brain atlas and growth model using diffeomorphic registration. In *International workshop on spatio-temporal image analysis for longitudinal and time-series image data*, pages 27–37. Springer.

Scott, J. A., Habas, P. A., Rajagopalan, V., Kim, K., Barkovich, A. J., Glenn, O. A., and Studholme, C. (2013). Volumetric and surface-based 3D MRI analyses of fetal isolated mild ventriculomegaly. *Brain Structure and Function*, 218(3):645–655.

Serag, A., Aljabar, P., Ball, G., Counsell, S. J., Boardman, J. P., Rutherford, M. A., Edwards, A. D., Hajnal, J. V., and Rueckert, D. (2012a). Construction of a consistent high-definition spatio-temporal atlas of the developing brain using adaptive kernel regression. *NeuroImage*, 59(3):2255–2265.

Serag, A., Aljabar, P., Ball, G., Counsell, S. J., Boardman, J. P., Rutherford, M. A., Edwards, A. D., Hajnal, J. V., and Rueckert, D. (2012b). Construction of a consistent high-definition spatio-temporal atlas of the developing brain using adaptive kernel regression. *Neuroimage*, 59(3):2255–2265.

Serag, A., Blesa, M., Moore, E. J., Pataky, R., Sparrow, S. A., Wilkinson, A., Macnaught, G., Semple, S. I., and Boardman, J. P. (2016). Accurate Learning with Few Atlases (ALFA): an algorithm for MRI neonatal brain extraction and comparison with 11 publicly available methods. *Scientific Reports*, 6(1):1–15.

Serag, A., Kyriakopoulou, V., Rutherford, M. A., Edwards, A. D., Hajnal, J. V., Aljabar, P., Counsell, S. J., Boardman, J., and Rueckert, D. (2012c). A multi-channel 4D probabilistic atlas of the developing brain: application to fetuses and neonates. *Annals of the BMVA*, 2012(3):1–14.

Simmons, A., Tofts, P. S., Barker, G. J., and Arridge, S. R. (1994). Sources of intensity nonuniformity in spin echo images at 1.5 T. *Magnetic resonance in medicine*, 32(1):121–128.

Sled, J. G., Zijdenbos, A. P., and Evans, A. C. (1998). A nonparametric method for automatic correction of intensity nonuniformity in MRI data. *IEEE transactions on medical imaging*, 17(1):87–97.

Smith, S. M. (2002). Fast robust automated brain extraction. *Human brain mapping*, 17(3):143–155.

Sowell, E. R., Thompson, P. M., Leonard, C. M., Welcome, S. E., Kan, E., and Toga, A. W. (2004). Longitudinal mapping of cortical thickness and brain growth in normal children. *Journal of neuroscience*, 24(38):8223–8231.

Tallinen, T., Chung, J. Y., Rousseau, F., Girard, N., Lefèvre, J., and Mahadevan, L. (2016). On the growth and form of cortical convolutions. *Nature Physics*, 12(6):588–593.

Thompson, D. K., Wood, S. J., Doyle, L. W., Warfield, S. K., Lodygensky, G. A., Anderson, P. J., Egan, G. F., and Inder, T. E. (2008). Neonate hippocampal volumes: prematurity, perinatal predictors, and 2-year outcome. *Annals of neurology*, 63(5):642–651.

Toro, R. and Burnod, Y. (2005). A morphogenetic model for the development of cortical convolutions. *Cerebral cortex*, 15(12):1900–1913.

Tourbier, S., Hagmann, P., Cagneaux, M., Guibaud, L., Gorthi, S., Schaer, M., Thiran, J.-P., Meuli, R., and Cuadra, M. B. (2015). Automatic brain extraction in fetal MRI using multi-atlas-based segmentation. In *Medical Imaging 2015: Image Processing*, volume 9413, page 94130Y. International Society for Optics and Photonics.

Tustison, N., Avants, B., Cook, P., Zheng, Y., Egan, A., Yushkevich, P., and Gee, J. (2010a). N4ITK: improved N3 bias correction. *Medical Imaging, IEEE Transactions on*, 29:1310 – 1320.

Tustison, N. J., Avants, B. B., Cook, P. A., Zheng, Y., Egan, A., Yushkevich, P. A., and Gee, J. C. (2010b). N4ITK: improved N3 bias correction. *IEEE transactions on medical imaging*, 29(6):1310–1320.

Twickler, D. M., Magee, K. P., Caire, J., Zaretsky, M., Fleckenstein, J. L., and Ramus, R. M. (2003). Second-opinion magnetic resonance imaging for suspected fetal central nervous system abnormalities. *American journal of obstetrics and gynecology*, 188(2):492–496.

Urru, A., Nakaki, A., Benkarim, O., Crovetto, F., Segales, L., Comte, V., Hahner, N., Eixarch, E., Gratacós, E., Crispi, F., Piella, G., and González Ballester, M. A. (2022). An automatic pipeline for atlas-based fetal and neonatal brain segmentation and analysis. *https://arxiv.org/abs/2205.07575*.

Van Leemput, K., Maes, F., Vandermeulen, D., and Suetens, P. (1999). Automated model-based tissue classification of MR images of the brain. *IEEE transactions on medical imaging*, 18(10):897–908.

Voorhies, W. I., Miller, J. A., Yao, J. K., Bunge, S. A., and Weiner, K. S. (2021). Cognitive insights from tertiary sulci in prefrontal cortex. *Nature communications*, 12(1):1–14.

Welker, W. (1990). Why does cerebral cortex fissure and fold? *Cerebral cortex*, pages 3–136.

Wolosin, S. M., Richardson, M. E., Hennessey, J. G., Denckla, M. B., and Mostofsky, S. H. (2009). Abnormal cerebral cortex structure in children with ADHD. *Human brain mapping*, 30(1):175–184.

Wright, I. C., Rabe-Hesketh, S., Woodruff, P. W., David, A. S., Murray, R. M., and Bullmore, E. T. (2000). Meta-analysis of regional brain volumes in schizophrenia. *American Journal of Psychiatry*, 157(1):16–25.

Wright, R., Kyriakopoulou, V., Ledig, C., Rutherford, M. A., Hajnal, J. V., Rueckert, D., and Aljabar, P. (2014). Automatic quantification of normal cortical folding patterns from fetal brain MRI. *Neuroimage*, 91:21–32.

Xue, H., Srinivasan, L., Jiang, S., Rutherford, M., Edwards, A. D., Rueckert, D., and Hajnal, J. V. (2007). Automatic segmentation and reconstruction of the cortex from neonatal MRI. *Neuroimage*, 38(3):461–477.

Yeo, B. T. T., Sabuncu, M. R., Vercauteren, T., Ayache, N., Fischl, B., and Golland, P. (2010). Spherical demons: fast diffeomorphic landmark-free surface registration. *IEEE Trans Med Imag*, 29(3):650–668.

Yun, H. J., Im, K., Yang, J.-J., Yoon, U., and Lee, J.-M. (2013). Automated sulcal depth measurement on cortical surface reflecting geometrical properties of sulci. *PloS one*, 8(2):e55977.